NATIONAL TRANSPORTATION SAFETY BOARD
Office of Research and Engineering
Materials Laboratory Division
Washington, D.C. 20594

February 2, 2023

MATERIALS LABORATORY FACTUAL REPORT Report No. 21-081

A. ACCIDENT INFORMATION

Place	:	Pine Grove, Oregon
Date	:	August 23, 2020
Vehicle	:	Kaman K-1200, N314
NTSB No.	:	WPR20LA283
Investigator	:	Fabian Salazar, ASI-WPR

B. COMPONENTS EXAMINED

1) Main rotor blades, rotor hubs, lead lag dampers, and flap brackets at wreckage location.
2) One servo flap fractured in two pieces; P/N: K915101-003; S/N: 0529A.
3) Bell crank with fractured input control rod and attached flap control rod.
4) Three sister flaps from the same aircraft; See below for P/N and S/N information.
5) Three sister flap control rods from the same aircraft.

C. DETAILS OF THE EXAMINATION

On August 24, 2020, at approximately 18:00 Pacific daylight time, a Kaman K-1200, N314, was substantially damaged when it was involved in an accident near Pine Grove, Oregon. Radio communications with the helicopter, which was conducting water bucket operations, was lost. The rotorcraft wreckage was subsequently found at a designated dip site on the White River. The pilot was fatally injured.

The K-1200 is equipped with two counterrotating, side-by-side, intermeshing rotors, with two blades per rotor for a total of four blades. The rotors are out of phase by 90° and are tilted outward to allow each blade to clear the opposing rotor hub. Viewed top down, the left rotor rotates in the counterclockwise direction and the right rotor rotates in the clockwise direction. An illustration of a main rotor blade assembly (left rotor) is shown in figure 1. The blade spar is manufactured from laminated spruce planks, the afterbody is manufactured from a honeycomb core material, and the blade is covered by a fiberglass composite skin. Blade pitch is controlled by a servo flap, which is attached to the blade by two attachment brackets at approximately STA 190 and STA 226 (The outboard tip of the blade is at approximately STA 289). The flap pivots about a spanwise axis of rotation. Flap pitch is controlled by a push/pull rod that attaches to the flap at its inboard end. When the flap is pitched leading edge down, aerodynamic forces on the flap cause the outboard end of the main rotor blade to twist to a leading edge up conformation (relative to neutral flap setting). Conversely, with the flap set to leading edge up, the

outboard end twists to a leading edge down conformation (also relative to neutral flap setting).

The left rotor blades and the afterbody of one of the servo flaps were located comparatively far away from the crash site. While one of the right rotor blades was located at the crash site (right-hand white) and pieces of the other blade (right-hand red) were located within 81 feet of the crash site, the left rotor blades were located 500 feet (left-hand red) and 560 feet (left-hand white) from the site. In addition, the afterbody of the left-hand white (LHW) servo flap had separated from its spar and was located 192 feet from the crash site.

The servo flaps and control rods were examined at the NTSB Materials Laboratory and the aircraft wreckage was examined in Prineville, OR on June 1 and June 2, 2021. Findings from the wreckage exam are presented first followed by findings from the laboratory exam of the fractured flap, sister flaps, and flap control rods. For more information on the wreckage exam, see the Airworthiness Group Factual Report.

1. Examination of aircraft wreckage

The scope of the wreckage exam for this report consists of the root end fractures of the left-hand main rotor blades, notable contact marks on the left and right rotor systems, status of the lead/lag dampers on the left rotor, and control rod contact marks on the servo flap attachment brackets. The blade designations and associated flap information are listed in table 1. The blades are referred to as left-hand white (LHW), right-hand red (RHR), etc. Blades on a rotor comprise a matched set and are given the same numerical serial number followed by either ‘A’ or ‘B’.

Table 1: Main rotor blade and servo flap pairings on the accident helicopter. The separated flap was located on the left-hand white MRB.

Main Rotor Blade (MRB)	MRB S/N	Flap P/N	Flap S/N	Direction of rotation (viewed top down)
Left-hand white	473A	K915101-003	0529A	Counterclockwise
Left-hand red	473B	K915101-003	0536A	Counterclockwise
Right-hand white	470A	K915101-004	0564A	Clockwise
Right-hand red	470B	K915101-004	0565A	Clockwise

a. Left rotor blade root fractures and rotor system contact marks

The inboard and outboard sides of the LHW main rotor blade root fracture are shown in figures 2 and 3, respectively. There were chordwise separations in the afterbody skin at approximately STA 65 and 75 and chordwise separations in the honeycomb core from trailing edge to leading edge between these stations as well. The spar was fractured in the same region. The aft portion of the spar fracture (see figures 3a and b) exhibited an oblique fracture morphology, alternating between inboard and outboard progression as the fracture transitioned between adjoining spar planks, extending outboard as far as STA 77.7. Approximately halfway across the spar, the fracture transitioned to progression

in the inboard longitudinal direction to approximately STA 67 after which it progressed in the chordwise direction along a comparatively flat path until intersecting the leading edge. The afterbody skin separation maintained its chordwise separation path across the jagged portion of the spar fracture and then followed the spar fracture along the longitudinal split and through the intersection with the leading edge. The features were consistent with a forward bending fracture.

Impact marks were observed on the lower surface of the LHW rotor blade as indicated in figure 2c. One mark, at approximately STA 63 was oriented in the chordwise direction, was approximately 2 inch wide, and exhibited a red stripe mark within the contact region, as shown in greater detail in figure 2d. Examination of the right rotor hub (figures 4a and 4b) indicated that the blade hinge pivots were painted with a white or red stripe and that the upper portion of the red paint stripe on the RHR hinge pivot had been rubbed off. Another mark at approximately STA 55 had fractured the lower skin and created an indent on the lower surface.

The inboard and outboard sides of the LHR main rotor blade root fracture are shown in figures 5 and 6, respectively. The inboard fracture was located between STA 47 and 48 (approx.). The wooden spar, as seen in figure 5b, appeared to be mechanically damaged, with multiple longitudinal splits, fragmented ends, and bent ends. The upper and lower blade surfaces on the outboard side of the root fracture are shown in figures 6a and 6b respectively and an oblique view of the spar fracture is shown in figure 7. On the outboard side, the spar fracture was located at approximately STA 57, leaving an approximately 9-inch to 10-inch length of the spar unaccounted for. Between STA 47 and 57, there was peel separation of the upper skin and lower skin. The outboard side of the spar fracture exhibited longitudinal splitting and fibrous features toward the aft and lower portion of the spar and exhibited flatter chopped fracture features closer to the leading edge and upper surface of the spar. The features were consistent with an upward bending fracture with possible additional forward bending.

There was a rub mark on the lower surface of the LHR blade, as indicated in figure 6b. The rub mark was roughly triangular in shape. The forward edge of the rub mark ran at an angle across the lower blade surface from the middle (chordwise) of the spar at STA 65.5 to the trailing edge at STA 83.5. The aft edge of the rub mark ran along the blade's trailing edge between STA 65.5 and STA 83.5. Inboard of STA 65.5 a strip of the lower skin was missing that was approximately in line with and at the same width and angle as the rub mark. Examination of the RHW (470A) rotor blade revealed a scuff and blunt impact mark along the leading edge of the blade between approximately STA 32 and STA 50, as shown in figure 8.

b. Left rotor lead/lag damper

The left rotor hub is shown in figure 9. The rotor blades are attached to the hub at hinge pins and pivot about their respective pins, leading or lagging as needed (within limits set by lead/lag stops). The leading side of each blade is connected to the trailing side of the opposite blade through lead/lag dampers. The damper consists of a piston that moves longitudinally inside a housing, with the piston and housing each connected

to a blade by a spherical bearing rod end. As the length of one damper shortens, the other damper lengthens. As shown in figure 9, the piston for the damper between the leading side of the LHR and the trailing side of the LHW blade had extended and pulled free of the housing. In contrast, the piston for the damper between the leading side of the LHW blade and the trailing side of the LHR blade was fully compressed and was separated from the rotor hub.

c. Inboard servo flap attachment brackets

Contact marks were observed on the inboard servo flap attachment brackets in line with the bolt head used to connect the servo flap control rod to the pitch change horn on the flap. Views of the inboard bracket for the LHW rotor blade are shown in figures 10a and b. The control rod was removed prior to the wreckage exam. The bracket for the LHR blade is shown in figures 11a and b and the RHW and RHR brackets are shown in figures 12a and 12b, respectively. Comparing figures 11, 12a, and 12b, the bolt head was aligned with the contact mark on the bracket when the rod was retracted (corresponding to a flap configuration of leading edge up).

All inboard brackets showed indications of contact along their lower outboard edge. The contact marks also extended from the lower edge along the side of the bracket, but to varying lengths. The mark on the LHW bracket, shown in figure 10b, extended approximately 0.60 inch up from the edge and the mark on the LHR bracket, shown in figure 11b, extended approximately 0.30 inch up from the edge. The marks on the RHR and RHL brackets extended approximately 0.16 inch and 0.07 inch from the edge, respectively.

2. Examination of separated servo flap

Several views of the separated servo flap from the LHW main rotor blade are shown in figures 13 and 14 (See table 1 above for part number and serial number information). The spar and afterbody are manufactured from plain weave, epoxy matrix, carbon fiber composite plies. An illustration of the flap spar-to-afterbody transition is shown in figure 15. The upper and lower afterbody skins consist of two plies each with a syntactic foam spacer between them. The skin plies lap and are bonded to the upper and lower surfaces of the spar. A C-channel ply is bonded to the aft face of the spar and to approximately 0.35 inch of the upper and lower afterbody skins. The inboard and outboard ends of the D-spar are capped by aluminum fittings. The inboard fitting (figure 14a) contains the pitch change horn for receiving the input from the pitch change control rod, a bearing surface for the spanwise pivot, and an enclosure for balance weights. The outboard fitting (figure 14b) contains the outboard bearing surface for the pivot. The inboard and outboard ends of the afterbody are capped by single-ply carbon fiber composite closeouts. The inboard closeout has a rounded, C-shaped, and tapered section profile while the outboard closeout is flat. The closeouts have tabs for bonding to the surrounding flap structure. The inboard closeout is bonded to the upper skin inner surface, lower skin inner surface, and aft face of the inboard aluminum attachment fitting. The outboard closeout is bonded to the upper skin inner surface, lower skin inner surface, and the aft face of the D-spar/channel ply.

The separation occurred generally at the spar-to-afterbody transition along the spanwise direction with some regions of peel separation. Along the lower surface, the two skin plies had fractured at or near the spar-to-afterbody transition and the channel ply exhibited peel separation from the spar along the entire spanwise length. An example of the peel separation is shown in figure 16 where the spar was sectioned at approximately STA 4.25.

The channel ply separated at different locations along the lower surface. Starting at the inboard end and for approximately 5 inch, the ply fractured at the transition bend between the lower skin and the spar. Outboard of this region, the channel ply separated from the spar along the edge of the peeled region, as shown in figures 17a and 17b, up to approximately STA 17 (approximately half the span width of the spar). In this region, the peel extended up approximately 0.42 inch up from the lower edge. Further outboard (figures 18 and 19), the channel ply transitioned to peel separation from the lower skin, up to approximately STA 29. The peel generally proceeded along the interface between the woven fibers of the channel ply and the interlayer resin. However, the fracture deviated into the resin as it progressed across several weft-aligned fiber tows, as indicated by the yellow arrows in figure 19. Fractographic examination of the resin fractures was consistent with fracture progressing outboard and toward the trailing edge. Outboard of STA 29 the peel ended and the channel ply fractured at the transition bend.

Along the upper surface, the afterbody skin plies initially fractured along the aft edge of the inboard fitting. Immediately outboard of the fitting, the plies began to peel from the spar, as seen in figure 13a and figure 20. The peel region extended approximately 3 inch in the spanwise direction and up to approximately 0.45 inch in the chordwise direction. Similar to the channel ply separation, fractographic examination indicated that the separation occurred primarily along the interface between the inner skin ply's woven fibers and the adjacent interlayer resin with occasional deviations into the resin as it encountered weft-aligned fiber tows. The resin fractures were consistent with the separation proceeding in the outboard direction. Outboard of this region, the skin plies had fractured at or near the spar-to-afterbody transition. Along the outermost 3.5 inch, the outer skin ply exhibited a small peel separation from the inner skin ply on the afterbody-side of the separation, as indicated in figure 13a. The peel extended up to approximately 0.25 inch the chordwise direction.

The channel ply had also peeled from the spar along portions of the upper surface. The primary region, seen in cross section in figure 16 at STA 4.25, started at the inboard end, gradually decreased in depth, and eventually ended at approximately STA 23. A secondary region was observed along the outermost 2 inches of the spar. Along the upper surface, the channel ply fractured primarily at the transition bend between the spar and the upper skin, with two exceptions: The first exception was between STA 19.5 and 21.5 (figure 21a), close to the end of the primary channel ply peel region. The fracture had moved down from the edge of the spar by a single transverse tow. The other region was associated with the secondary peel region (figure 21b) at the outboard end of the flap. Two inches from the end, the overlaid warp tows had peeled from the spar and fractured down from the edge by a single transverse tow. The fracture gradually moved down the

spar as it progressed outboard, extending down two tows from the edge at the outboard end of the spar.

The inboard and outboard closeout fitting bonding tab separations are shown in figures 22 and 23, respectively. As indicated in figure 22b, the bonding tab on the inboard closeout was missing. As seen in figure 22a and figure 24, a green epoxy adhesive and a piece of scrim cloth were used to bond the closeout tab to the aluminum fitting. Much of the area appeared to be unbonded. The adhesive exhibited a smooth and shiny appearance and the diamond pattern from the scrim cloth was visible underneath the adhesive. In some areas, the surface exhibited a dark brown color with a plain weave surface texture that was consistent with a remnant layer from the bonding tab. Around the perimeter of the bonding region, the adhesive had undergone cohesive fracture. The total area and bonded area (cohesive and peeled regions) on the aft face of the fitting were measured on a calibrated image and were approximately 0.871 inch^2 and 0.227 inch^2, respectively. The outboard closeout bonding tab, shown in figures 23a and 23b, was also largely unbonded. The total area and bonded area were approximately 1.227 inch^2 and 0.194 inch^2, respectively.

Crack propagation features in the fractured adhesive were used to trace the fracture path around the perimeter back to an origin at the lower inboard location of the bonding region. Figure 24 is annotated with yellow arrows indicating local directions of crack propagation as determined by radiating lines and curved crack arrest marks. Along the lower edge of the bonding region, lines radiated downward and outboard. Along the inboard edge, lines and crack arrest marks were consistent with a crack progressing from the lower side toward the upper side of the fitting. The features traced back to an origin area at the lower inboard region of the perimeter, shown in figures 25a and b. Here the adhesive formed a layer approximately 0.08 inch across, with the outer surface of the flap on one side and the inner cavity of the bonding region on the other. Fracture lines radiated from the inward-facing side of the layer initiating at or near the interface with the carbon fiber bonding ply (figure 25a). Along one half of the origin, the fracture proceeded along the adhesive/ply interface. Along the other half, the fracture diverted away from the interface, starting as a cohesive fracture through the adhesive. The cohesive fracture progressed approximately 0.04 inch across the adhesive layer before diverting into and continuing along the adhesive/ply interface. The crack progressed away from the origin along two fronts. One front progressed outboard along the lower surface to the lower edge of the afterbody. The other front progressed up along the inboard side, then outboard across the upper surface to the upper edge of the afterbody.

The outboard closeout was cracked along the upper and lower edges of the bond line with the afterbody as seen in figures 26a and b. The crack along the lower edge started near a midbody I-beam stiffener and progressed forward and aft approximately 1 inch, arresting before reaching the spar or trailing edge. Along the upper edge, a crack also extended forward and aft of the I-beam and a closeout tab that was bonded to the forward portion of the upper afterbody skin was missing. The tab had peeled from the skin leaving adhesive and carbon fiber ply imprints behind. Examination of the delamination

surface indicated that the tab delamination proceeded inboard and toward the leading edge, as indicated in figure 26c.

The spar / afterbody fracture was examined using a scanning electron microscope (SEM) with a focus on the fractured carbon fibers. Figure 27 shows an overview scan of the afterbody-side of the lower skin separation at the inboard end of the afterbody. Figures 28a – d show the afterbody and spar sides of the outer ply fracture at low and high magnification, respectively. On the spar side, the fiber fractures exhibited radial lines leading to chop marks (figure 28d) that were consistent with downward bending/buckling of the fibers. The fibers immediately adjacent to this region were also bent/buckled down. On the afterbody side (figure 28c), the fiber fractures closest to the interior of the flap exhibited radial lines consistent with tensile fractures, while closer to the outer (lower) surface, the corresponding fibers were not visible. As seen in figure 28b, the fracture plane in the region of buckled/bent fibers on the spar-side was offset from the adjacent fracture and most of the buckled/bent fiber fragments between the spar-side and afterbody-side fractures were missing. An additional cluster of buckled/bent fibers was located further outboard (figure 28a) and there were fiber fragments embedded in the fracture surface. Elsewhere along the spar / afterbody separation, fibers exhibited radial lines, consistent with tensile fractures, with occasional clusters of fibers exhibiting chop mark features, consistent with bend/buckle fractures. Fiber fragments and debris were often observed, consistent with fracture face contact. Several examples are shown in figures 29a – c. Along the lower skin and starting at approximately STA 2.00, most of the inner ply warp tows exhibited peel separation along their lower (outward) face (figures 30a and b). At approximately STA 28.5 the lower skin fracture shifted toward the leading edge by approximately 0.06 inch (figure 31) and the peel transitioned to transverse fractures across the inner ply tows (figures 32a and b) up to the outboard end of the flap.

The missing bonding tab's separation from the inboard closeout was also examined by SEM as shown in figure 33. The fractured fibers exhibited rubbing and the surface was covered by debris.

3. Pitch change control rod examination

The servo flap pitch change control rod, bellcrank, and fractured ends of the input control rod (internal to the main rotor blade along the spanwise direction) are shown in figure 34a (shown in an arbitrary configuration). The input control rod was fractured near the inboard and outboard ends. The fractures exhibited necking and slanted fractures, consistent with overstress. The bellcrank exhibited a contact mark, indicated in figure 34b, consistent with contact by the rod end at the base of the servo flap control rod. Visual examination of the servo flap control rod indicated that the rod was bent, as shown in figure 35a. The other rods were removed from the aircraft and are shown in figures 35b – d.

Several measurements were made on each rod. The bend angle of each rod and each rod end clevis was measured using a structured light 3D scanner (see the control rod example in figure 36). The rod outer diameter (OD) was measured using a micrometer and the inner diameter was measured using a split ball gauge / micrometer. The hardness

of each rod was measured with a Rockwell hardness tester in accordance with standard laboratory procedures. The results are shown in table 2. The bend angles for the control rods were 2.2°, 0.6°, 0.0°, and 0.1° for the LHW, LHR, RHW, and RHR flaps, respectively. The bend angles of the rod end clevises were 0.4°, 0.6°, 0.6°, and 0.6° for the LHW, LHR, RHW, and RHR flaps, respectively. The dimensional and hardness attributes met the manufacturer's requirements.

Table 2. Bend angles, dimensions, and hardness measurements on the servo flap control rods.

Flap ID	Bend Angle - Rod, deg	Bend angle – Rod end clevis, deg	Rod ID, inch	Rod OD, inch	Hardness, HRC
LHW	2.2	0.4	0.2621, 0.2623	0.3385	35.8
LHR	0.6	0.6	0.2620, 0.2624	0.3387	37.5
RHW	0.0	0.6	0.2620	0.3386	36.5
RHR	0.1	0.6	0.2637	0.3380	39.7

4. Sister flap inboard closeout examination

The sister flaps from the accident aircraft were examined for visual signs of cracks, particularly around the inboard closeout and the bond between the closeout and aluminum fitting was evaluated. Overview images of the LHR, RHW, and RHR servo flaps are shown in figures 37a – c, respectively. The RHR flap had indications of foreign body contact on the outboard portion of the upper skin between STA 25 and 30. All flaps exhibited cracking along the bond line between the closeout and the aluminum fitting, but the extent of cracking varied. The LHR flap inboard closeout exhibited a hairline crack that extended approximately 1 inch along the upper surface and halfway down the inboard side of the flap, as seen in figure 38. The RHW inboard closeout cracks extended approximately 1 inch along the upper surface, wrapped around the inboard side, and extended approximately 0.6 inch along the lower surface, as seen in figures 39a – c. The RHR inboard closeout cracks extended approximately 0.5 inch along the upper surface, wrapped around the inboard side along the bond line, and extended approximately 1.7 inch along the lower surface, as seen in figures 40a – c. The closeout had sustained damage as seen in figure 40b. There were holes through the upper and lower surfaces and the closeout was partially fractured between the holes. The inboard ends of the flaps were sectioned as described below. The RHR flap was cut along the red dashed line in figure 40c, which passed through a crack along the underside of the flap. The cross section through the crack, shown in figure 40d indicated that the outer and inner skin plies were fractured beneath the surface crack.

Additional damage was observed at the outboard end of the RHR servo flap. The outboard closeout had cracked along the upper and lower bond lines (figure 41a). The cracks started near the mid-afterbody I-beam and extended forward and aft. The lower afterbody skin was cracked in the spanwise direction at the outboard end (figure 41b). One crack coincided with the trailing face of the D-spar and the other crack coincided with the forward end of the trailing edge strip.

The bond between the inboard aluminum fitting and the bonding tab on the inboard closeout was evaluated on cross sections through the bond for the sister flaps. The inboard ends of each flap were sectioned, as shown for the RHR flap in figure 42a. Figure 42b shows a view inside the cut end with labels for the bonding tab, aluminum fitting, and spar. The closeout cavity was filled with a slow cure epoxy, the flap piece was cut down as required, and the closeout was sectioned using a wet abrasive saw down the midline of the bond, as indicated in figures 42a and b. The cross section through the LHR servo flap closeout bond is shown in figure 43 and the cross sections through the RHW and RHR bond are shown in figures 44a and b, respectively. All bonds exhibited voids along the bond line. The relative fraction of voids was compared by measuring the total bond line length along the cross section, measuring the length of voids along the line, summing the void lengths, and calculating the ratio of total void length to total bond line length (see figure 45 for an example of void length measurement).[1] A similar measurement was performed on the LHW servo flap, but on a plan view image of the closeout fracture. The void length ratios for the LHW, LHR, RHW, and RHR servo flaps were 0.827, 0.563, 0.517, and 0.751, respectively.

Donald Kramer, Ph.D.
Sr. Materials Engineer

[1] The bond line measurements are for comparison purposes only.

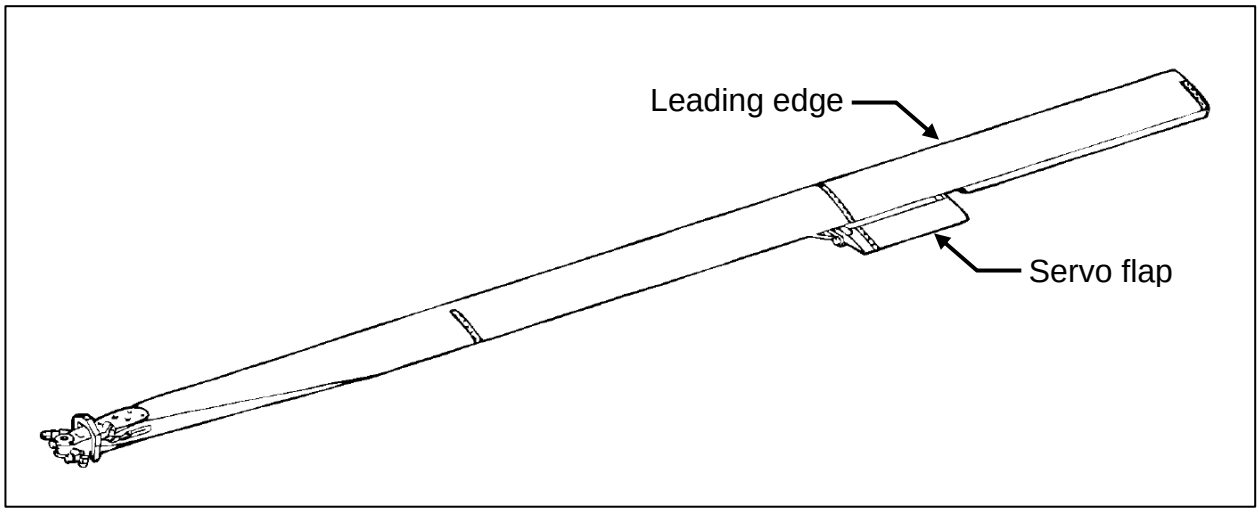

Figure 1. Illustration of a left rotor main rotor blade assembly with servo flap attached behind the trailing edge.

a)

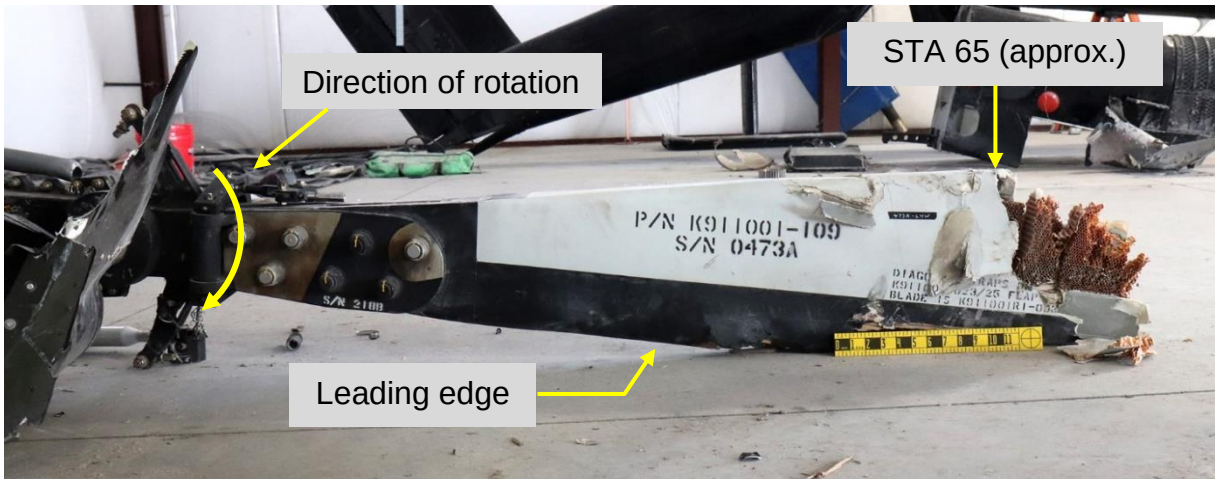

b)

Figure 2. Root end of the left hand white (LHW) main rotor blade (473A): a) view of the lower blade surface; b) view of the upper blade surface;

c)

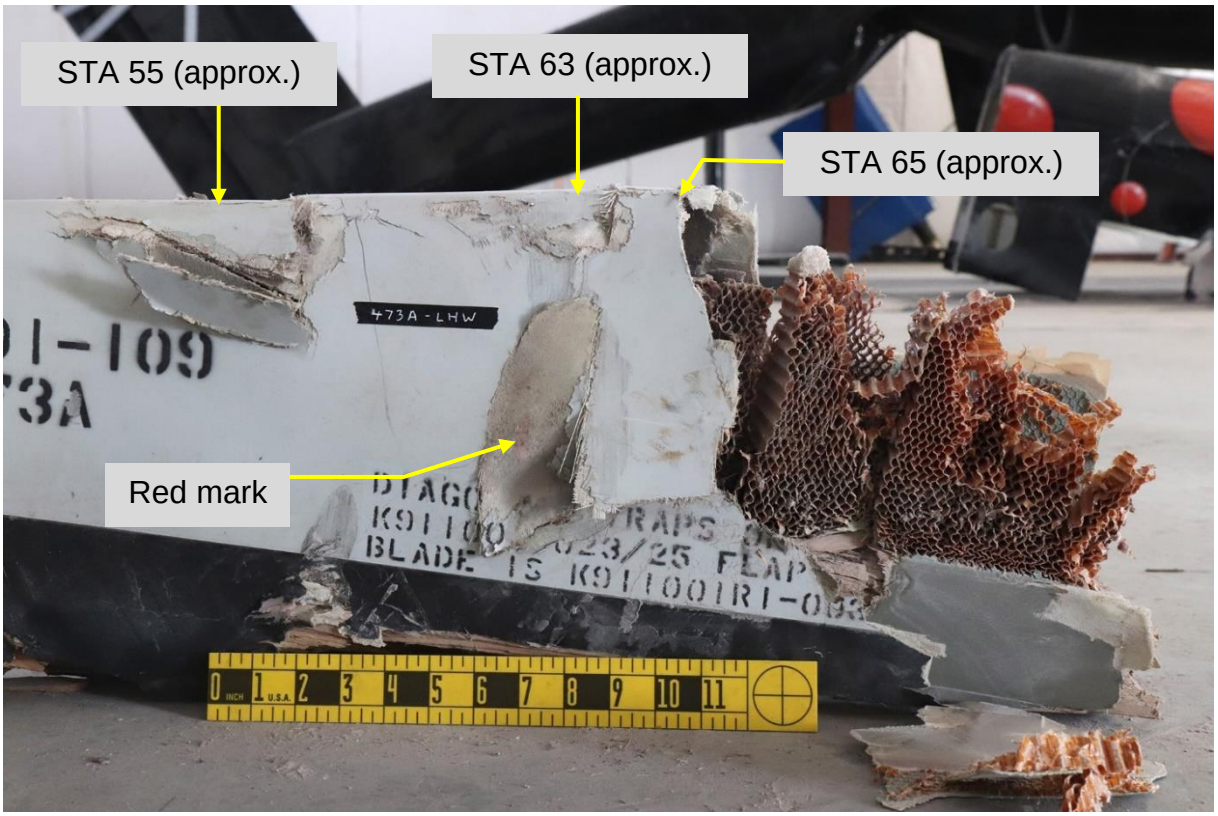

d)

Figure 2 (cont.). c) image near the separation showing rub and impact marks; and d) higher magnification image of the chordwise rub mark at STA 63 with a red mark indicated.

a)

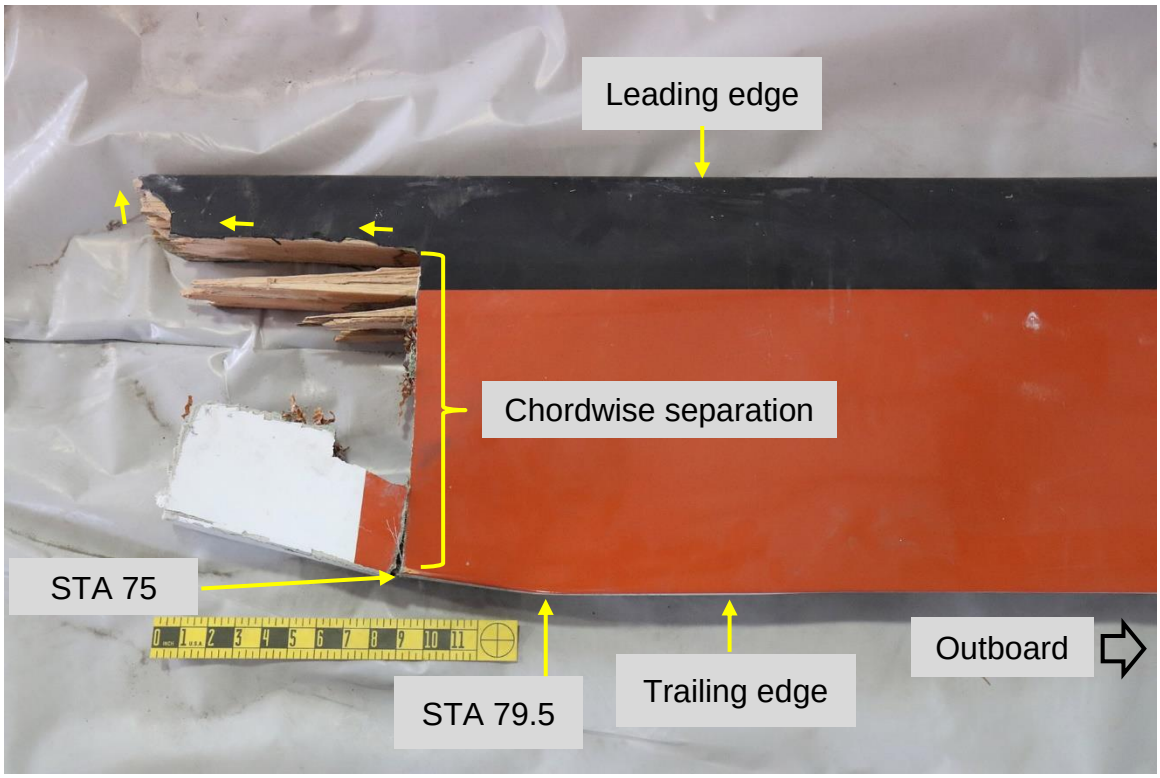

b)

Figure 3. Outboard side of LHW (473A) main rotor blade root fracture: a) Overview image of the upper side and b) closer view of the spar fracture.

a)

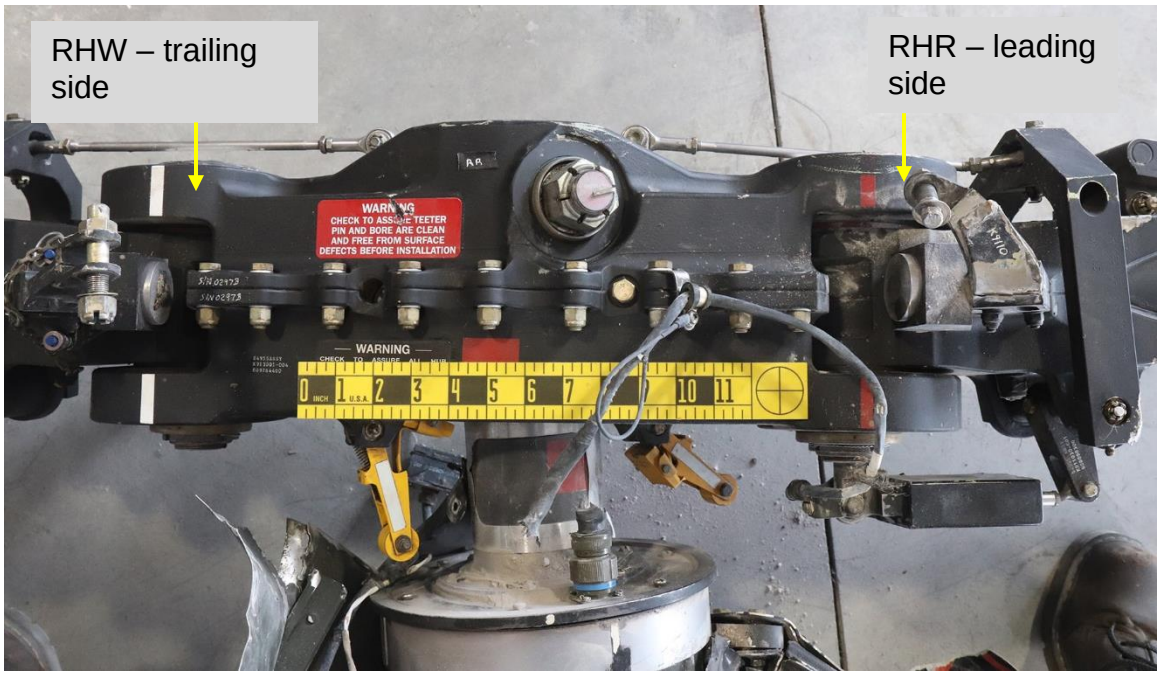

b)

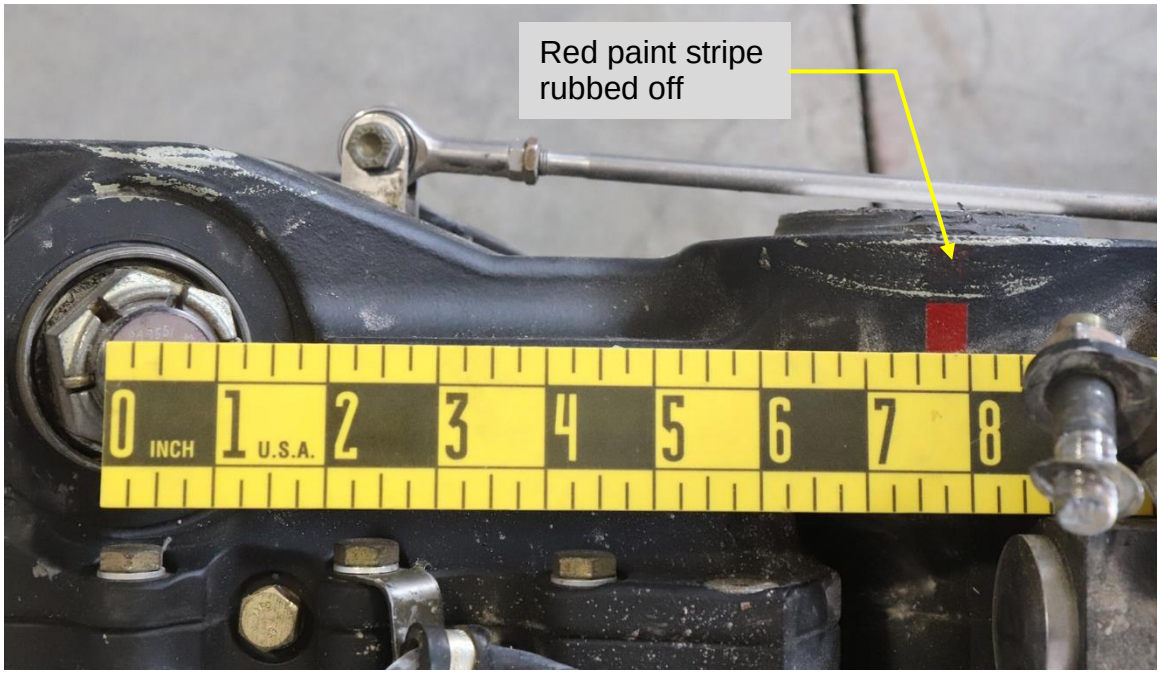

Figure 4. a) Image of the right rotor hub. The white blade (left side) rotates into the page and the red blade (right side) rotates out of the page; b) image indicating where the red paint stripe had been rubbed off the hub's red blade hinge pivot.

Figure 5. Images of the LHR (473B) main rotor blade root: a) view of the lower blade surface and b) view of the fractured spar.

a)

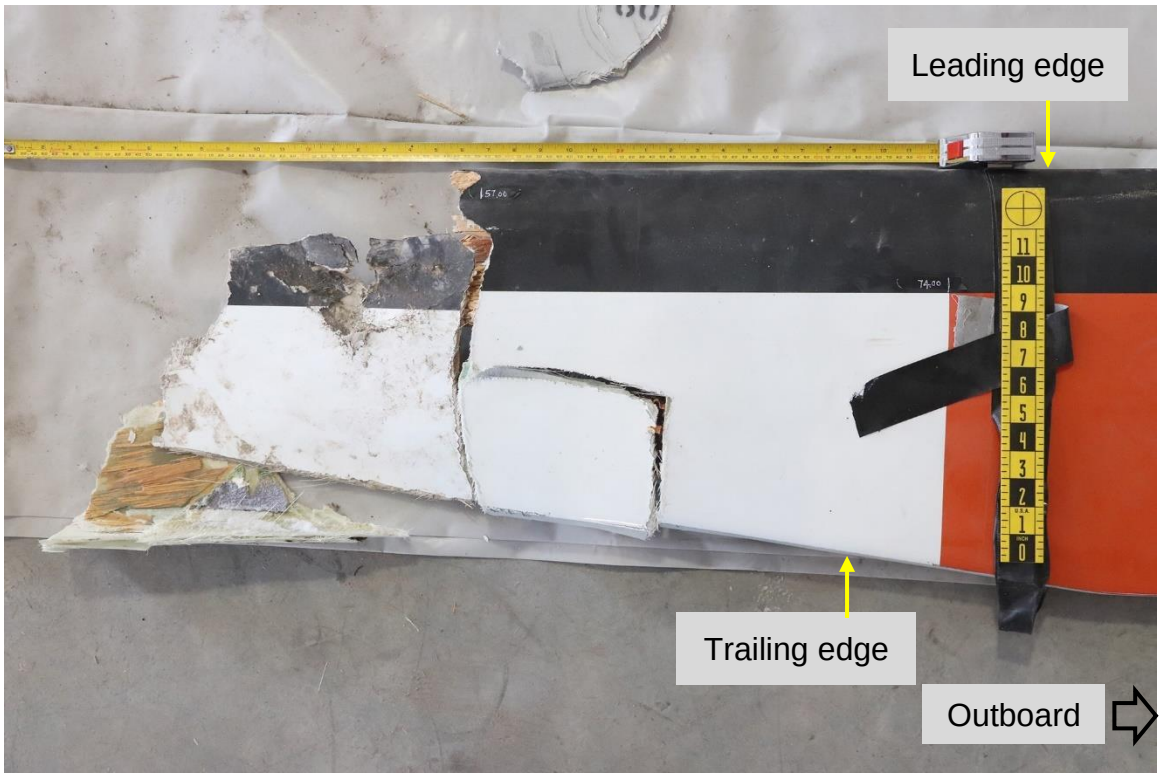

b)

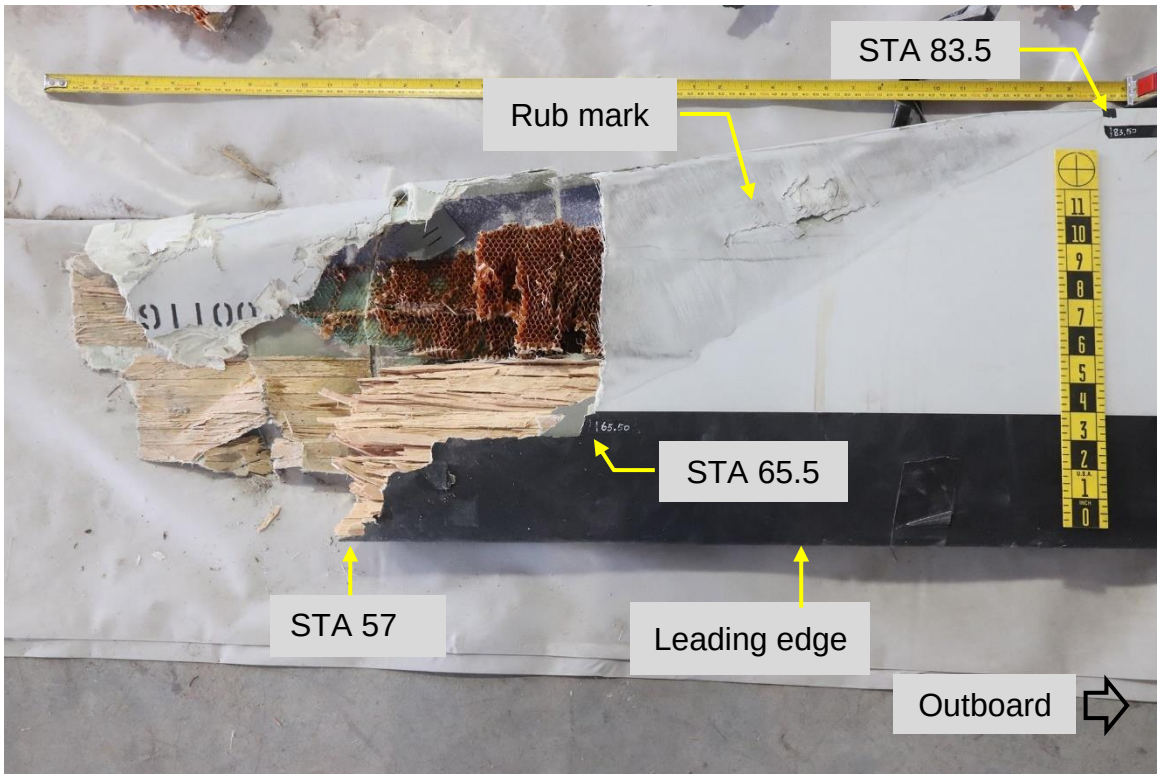

Figure 6. Images of the outboard side of the LHR (473B) blade root fracture: a) upper surface and b) lower surface.

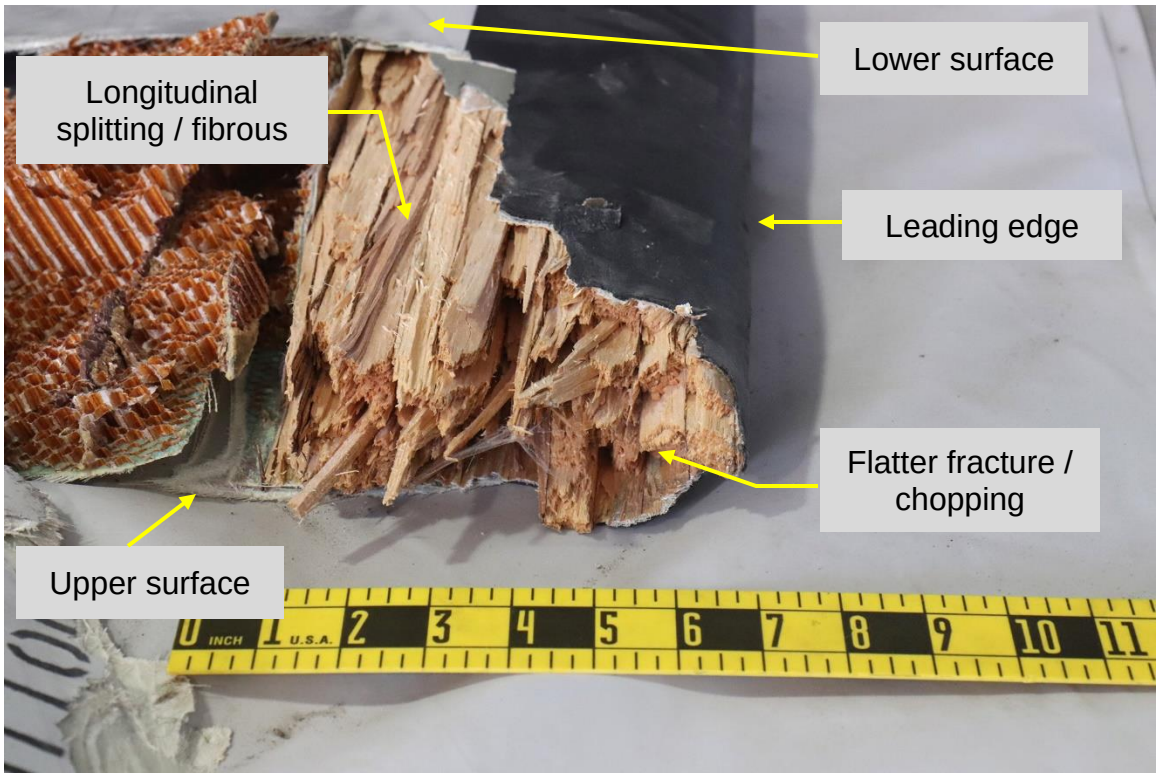

Figure 7. Image of the outboard side of the LHR blade spar fracture.

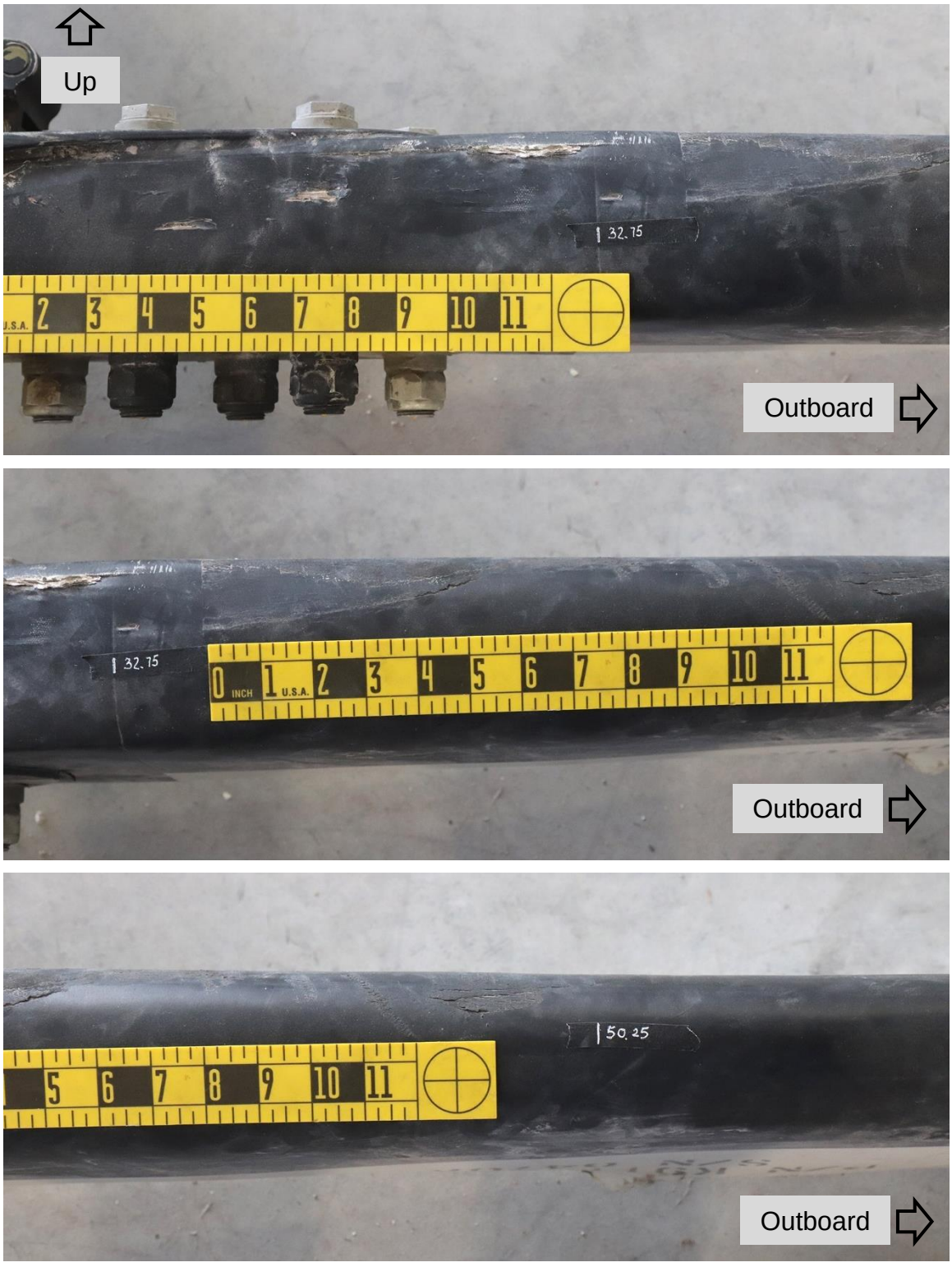

Figure 8. Scuff and impact marks along the leading edge of the RHW (470A) main rotor blade.

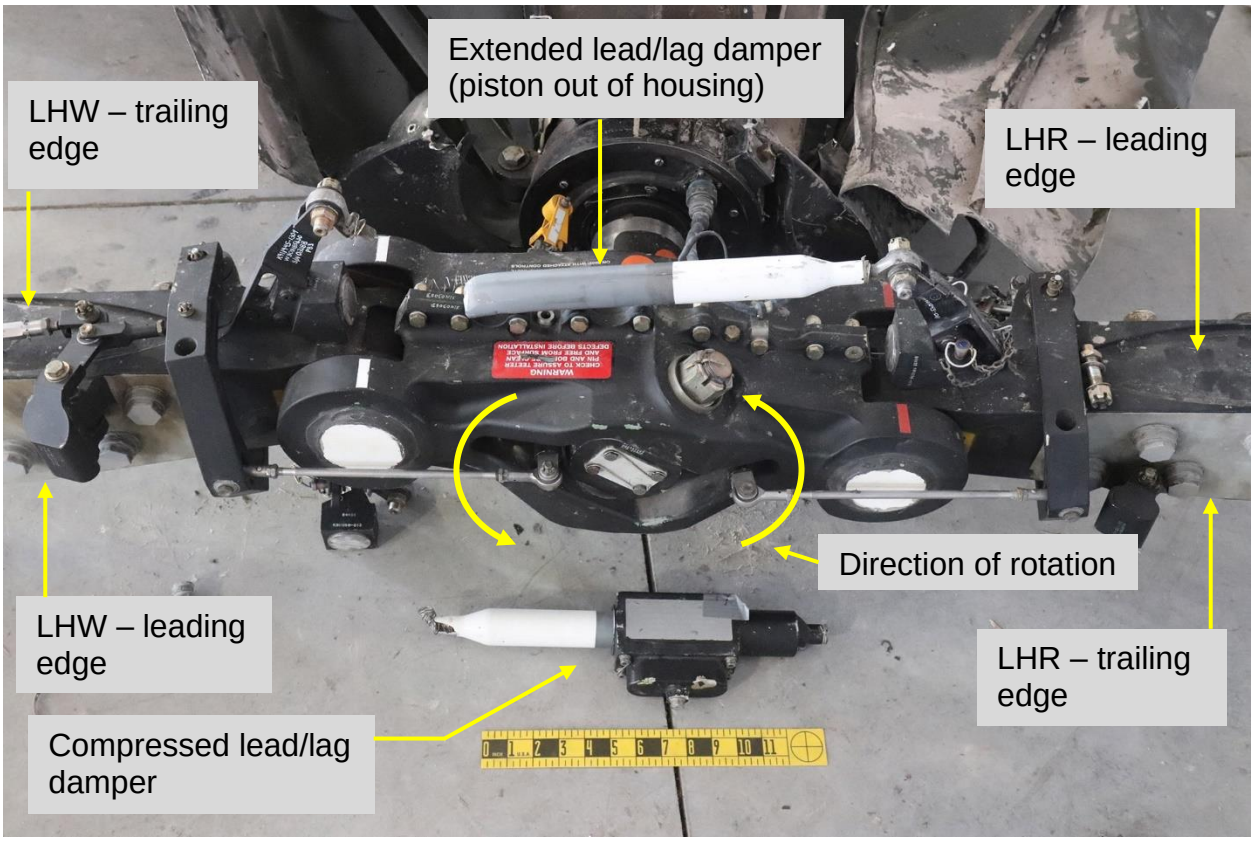

Figure 9. Image of the left rotor hub and lead / lag dampers. The damper connecting the leading edge of the LHR blade to the trailing edge of the LHW blade was extended and the piston had separated from the housing. The damper connecting the leading edge of the LHW blade to the trailing edge of the LHR blade was compressed.

a)

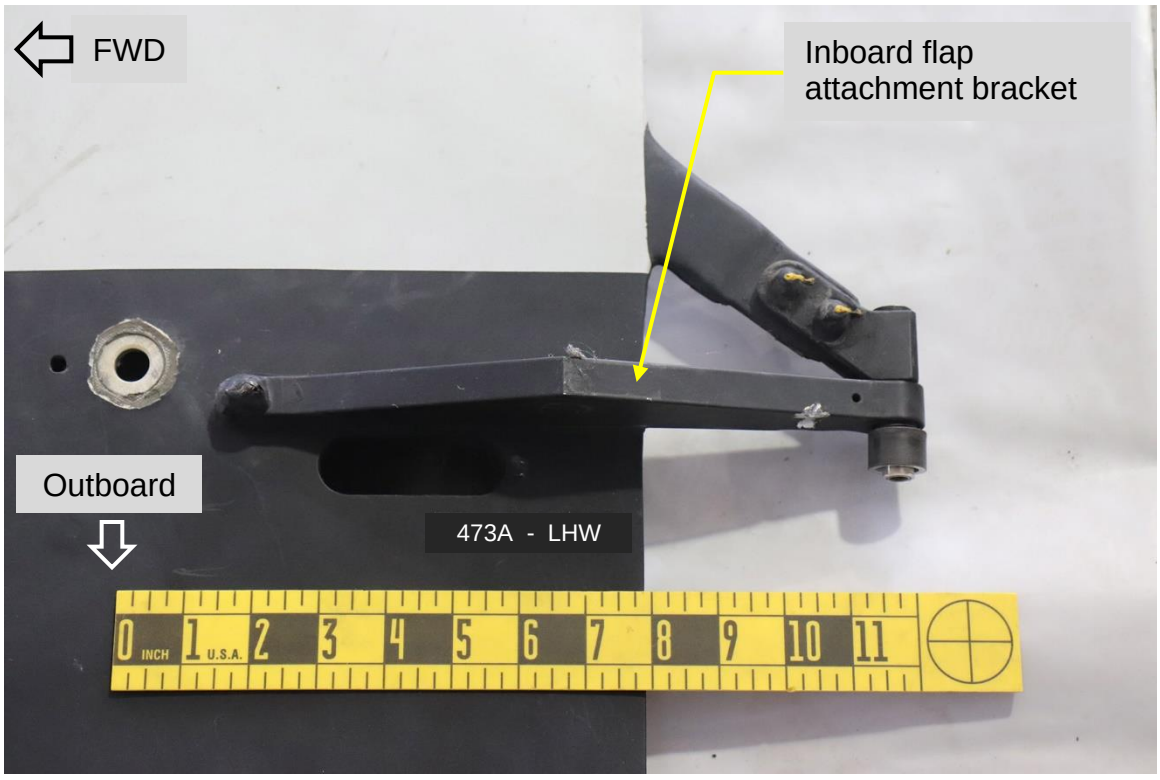

b)

Figure 10. Inboard flap attachment bracket for the LHW servo flap: a) View of lower blade surface and b) view of contact marks on inboard bracket.

a)

b)

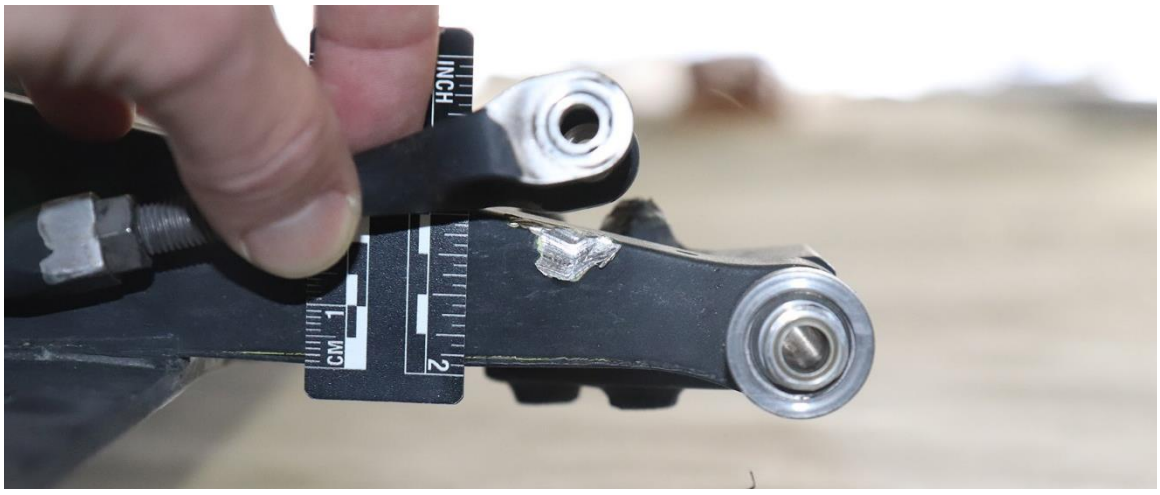

Figure 11. Inboard flap attachment bracket for the LHR servo flap: a) View of lower blade surface and b) view of contact marks on inboard bracket.

a)

b)

Figure 12. Views of contact marks on the right-hand rotor inboard flap attachment brackets: a) RHW and b) RHR.

a)

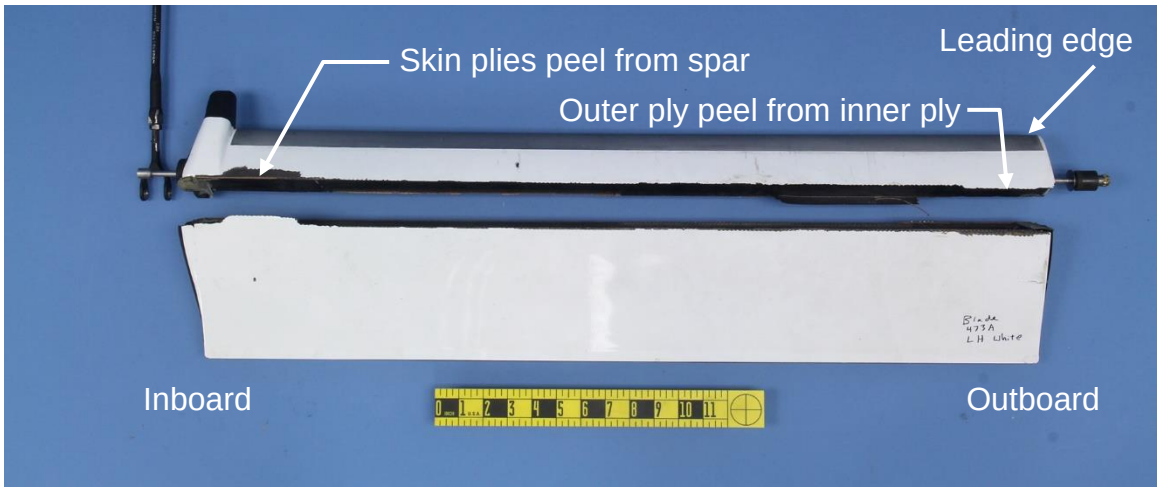

b)

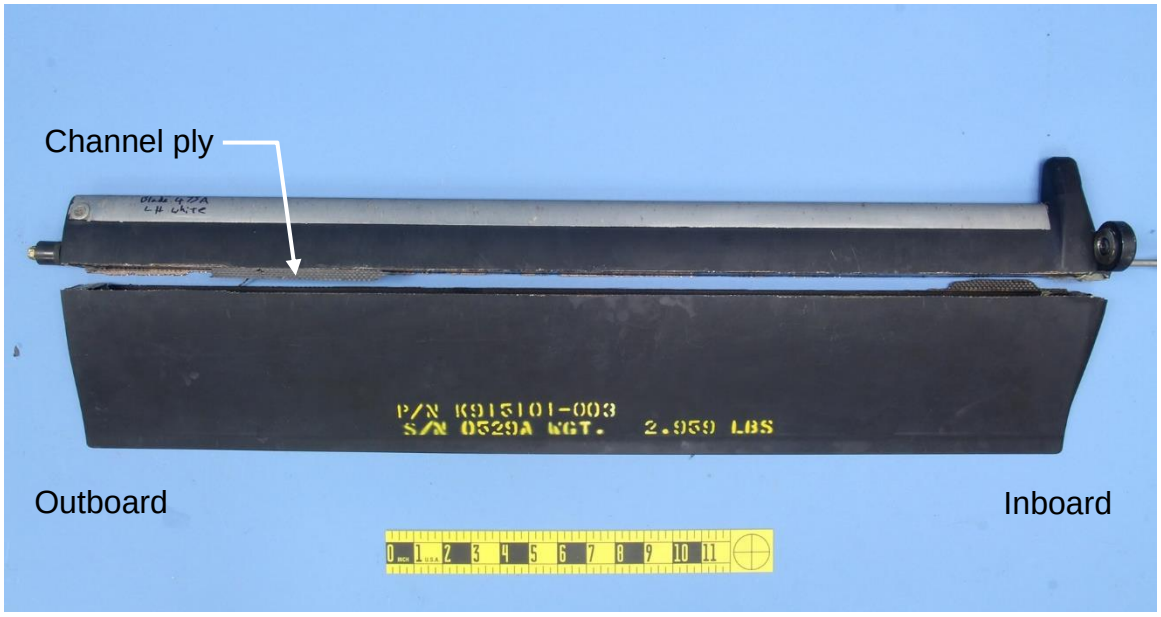

Figure 13: Separated servo flap assembly from the left rotor / white main rotor blade (LHW - Blade 473A), as received: a) view of the flap upper side and b) view of flap lower side.

a)

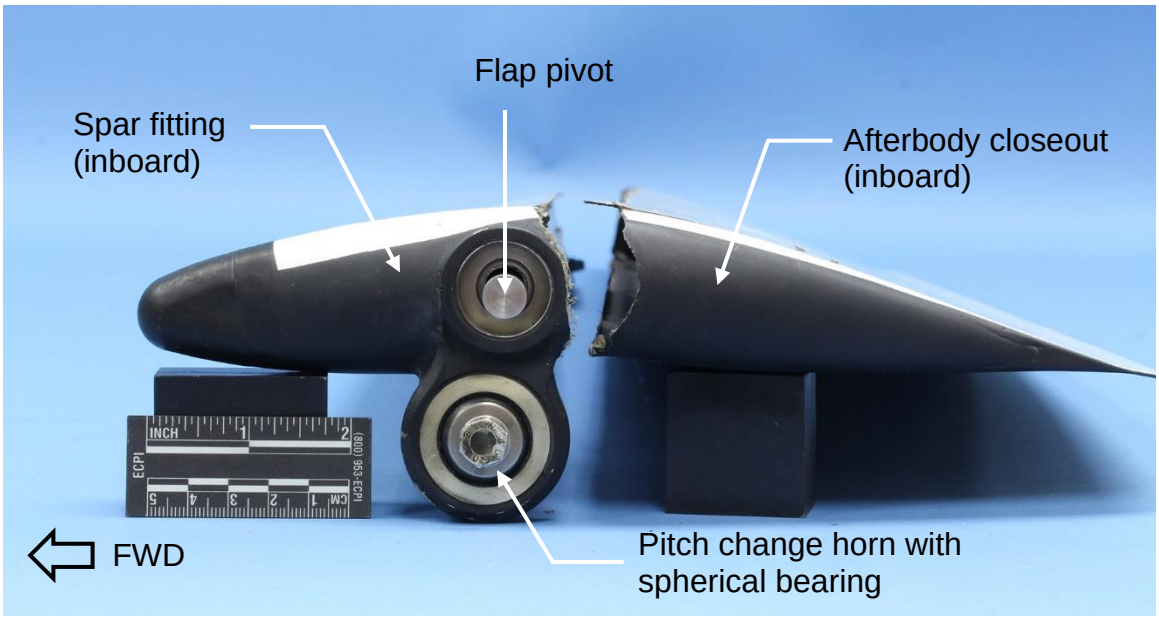

b)

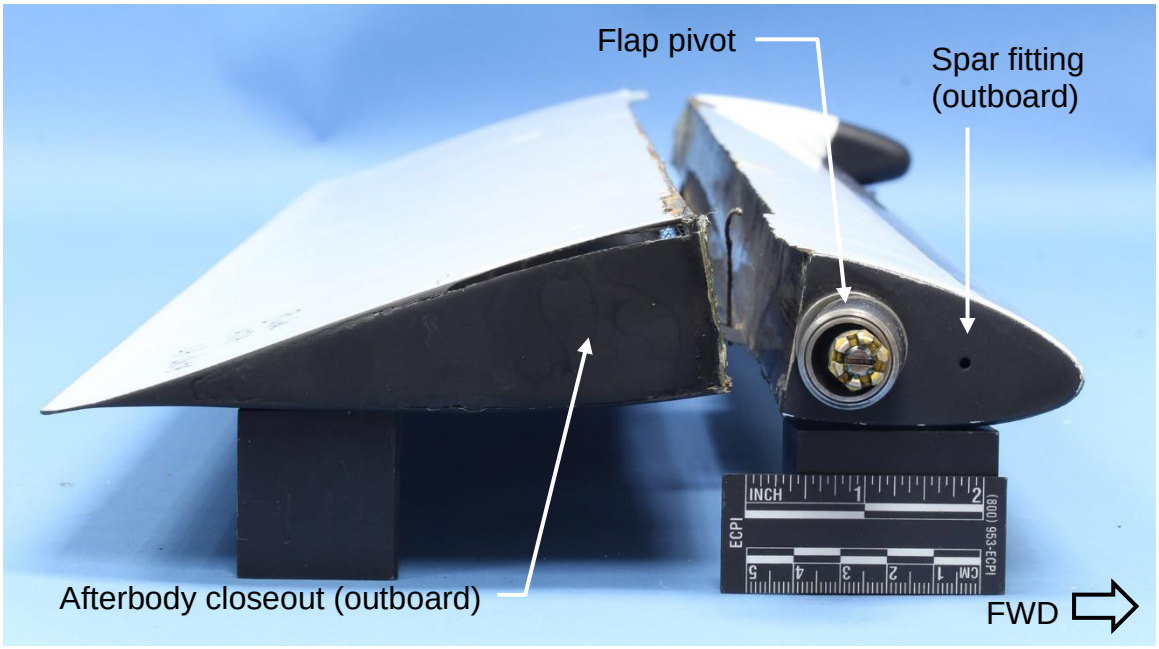

Figure 14. End views of the separated servo flap: a) inboard end viewed looking outboard and b) outboard end viewed looking inboard.

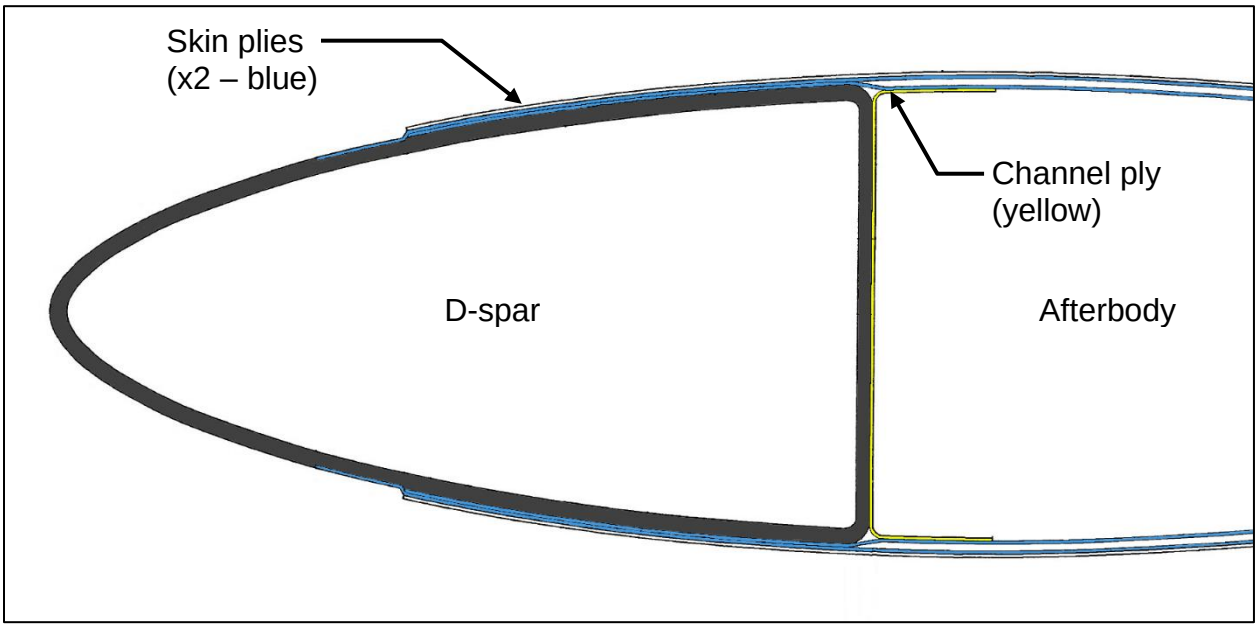

Figure 15: Cross section illustration of the servo flap at the spar-to-afterbody transition.

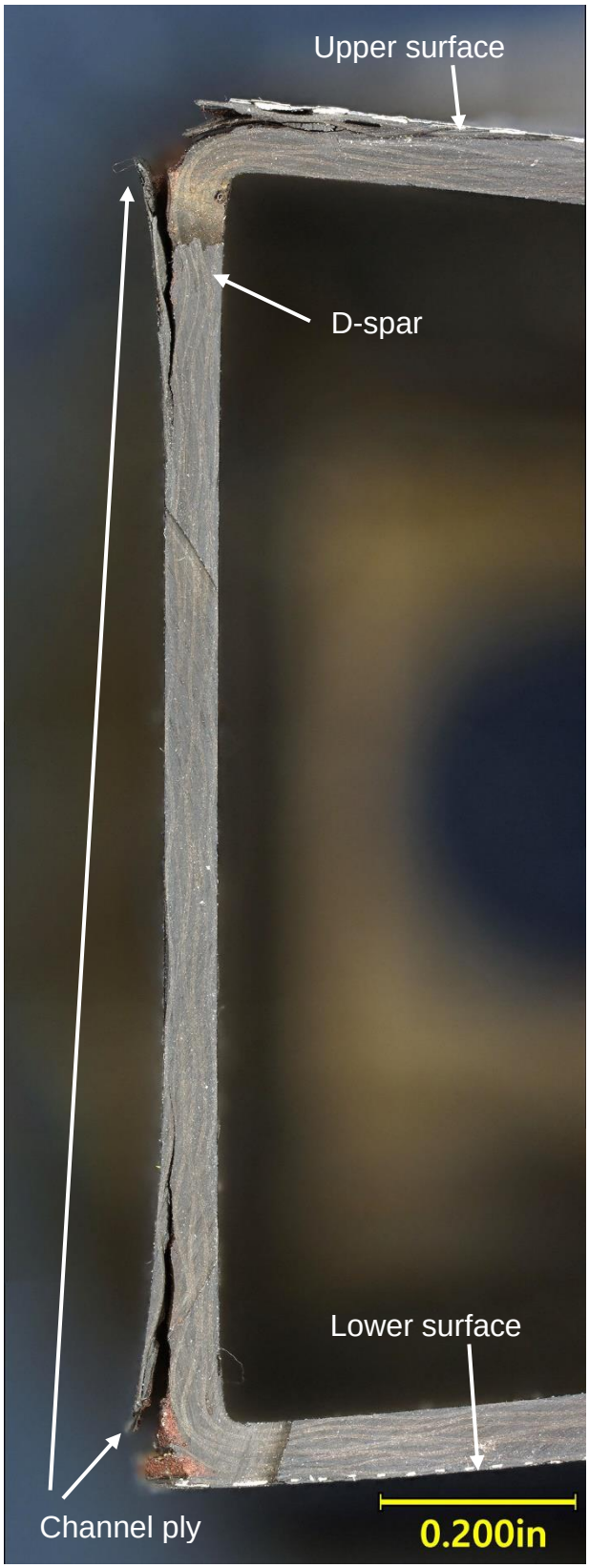

Figure 16. Cross section through spar at approximately STA 4.25 showing peel separation and fracture of channel ply. The view is looking inboard.

a)

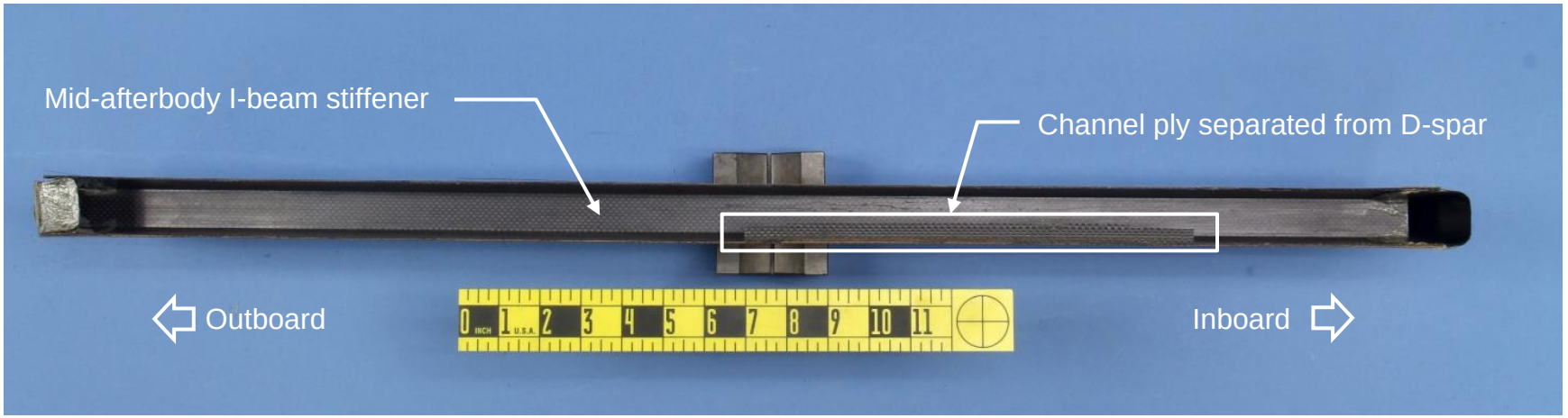

b)

Figure 17. a) Image of the separated servo flap afterbody viewed from the forward direction looking aft and b) image of the servo flap spar / channel ply aft face with portion of C-channel ply peel separated from spar.

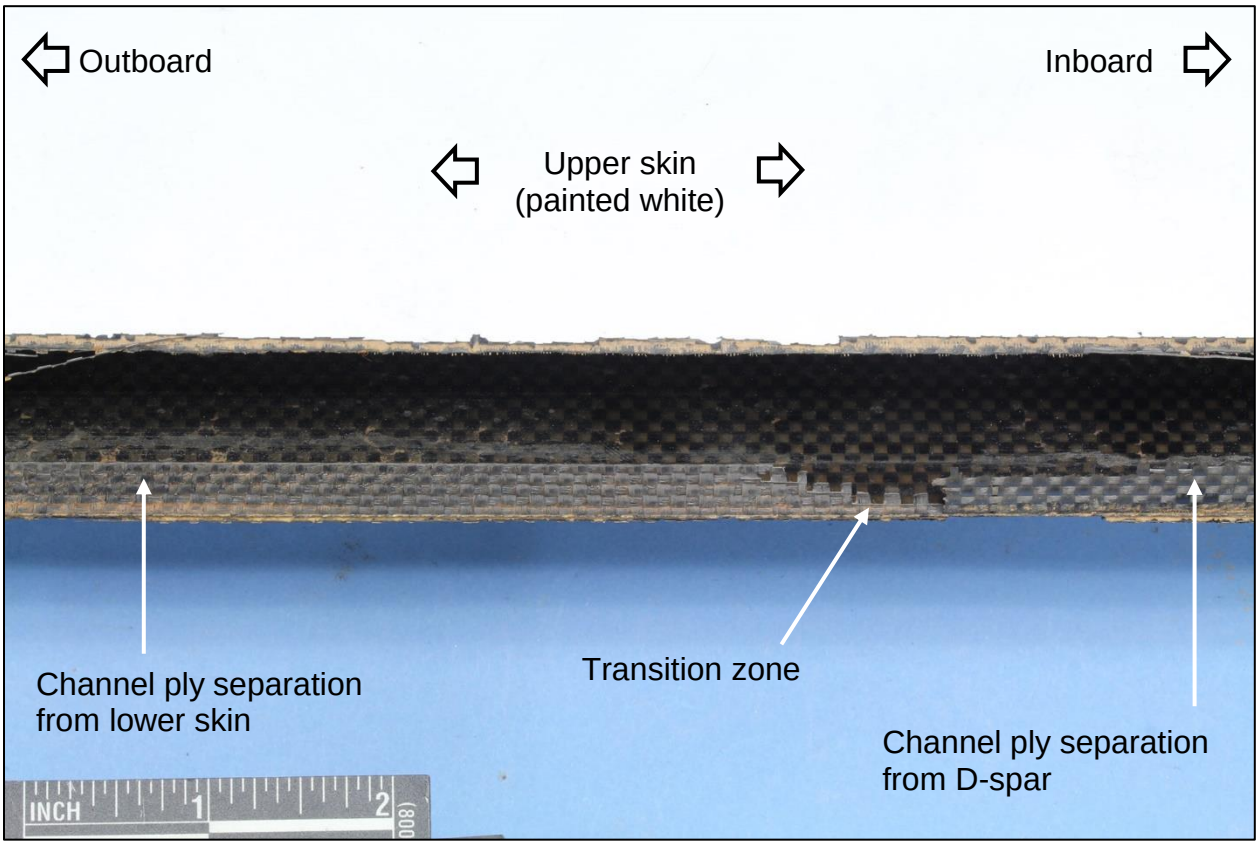

Figure 18. Image of afterbody near the middle (spanwise) where the channel ply transitioned from peel separation from the spar to peel separation from the lower skin.

Figure 19. Image showing channel ply peel separation from the lower afterbody skin. Yellow arrows indicate the local direction of crack progression.

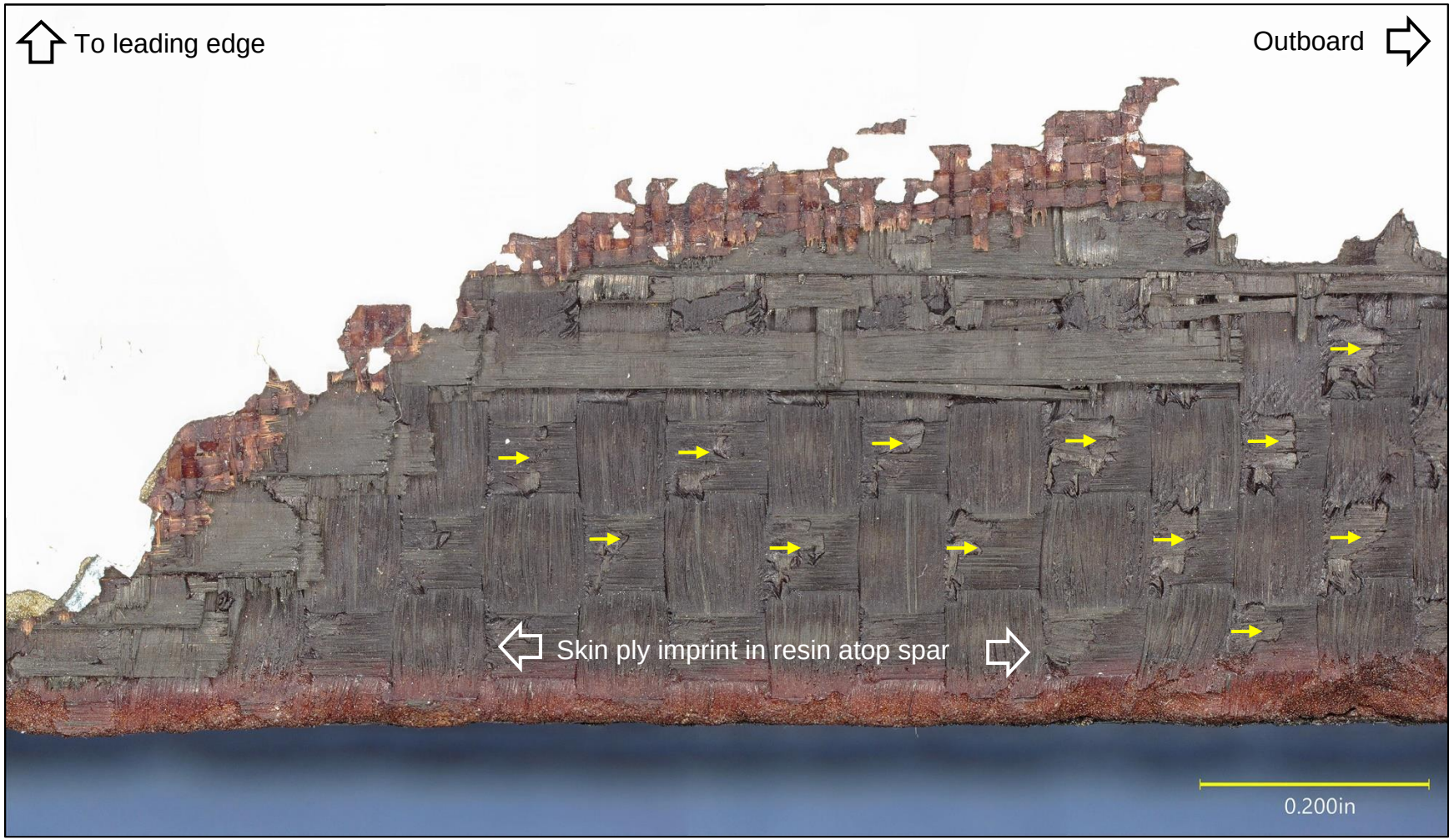

Figure 20. Image showing upper skin peel separation from inboard region of spar. Yellow arrows indicate the local direction of crack progression.

a)

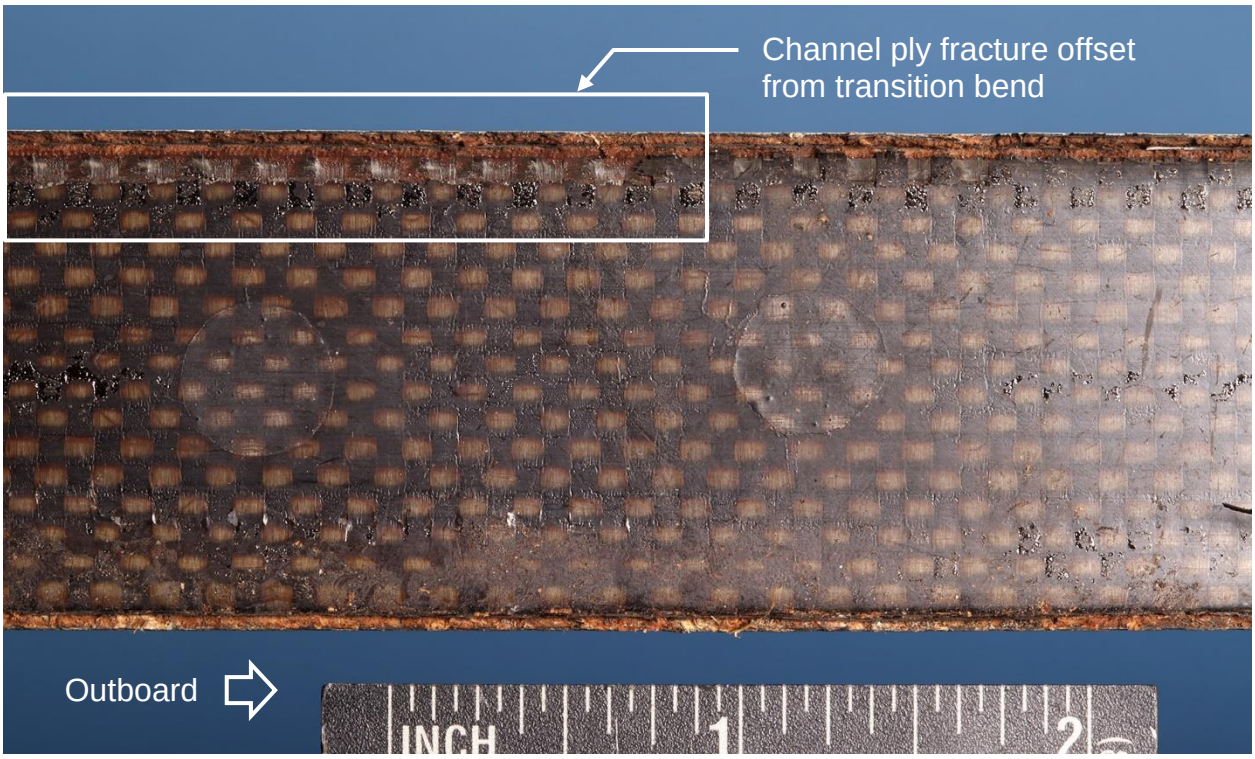

b)

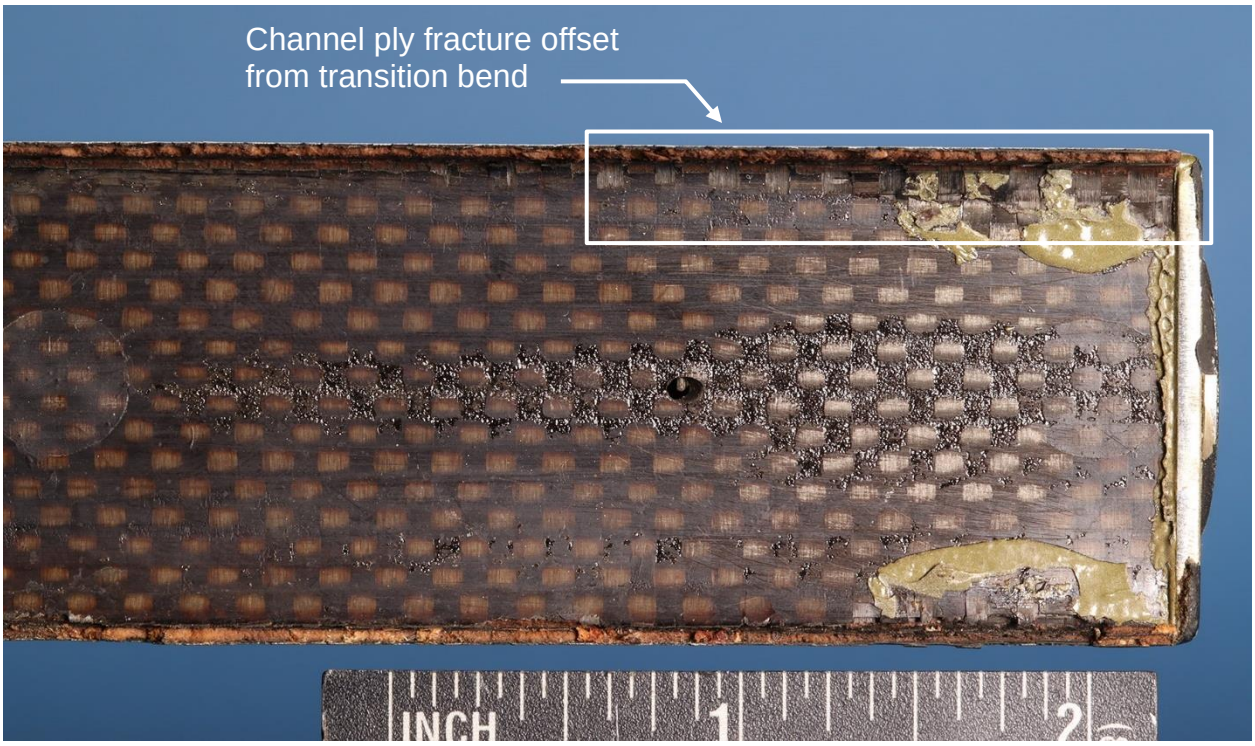

Figure 21. Images of the spar aft face showing regions where the upper channel ply fracture deviated from the transition bend: a) region between STA 19.5 and STA 21.5 and b) region near outboard end.

a)

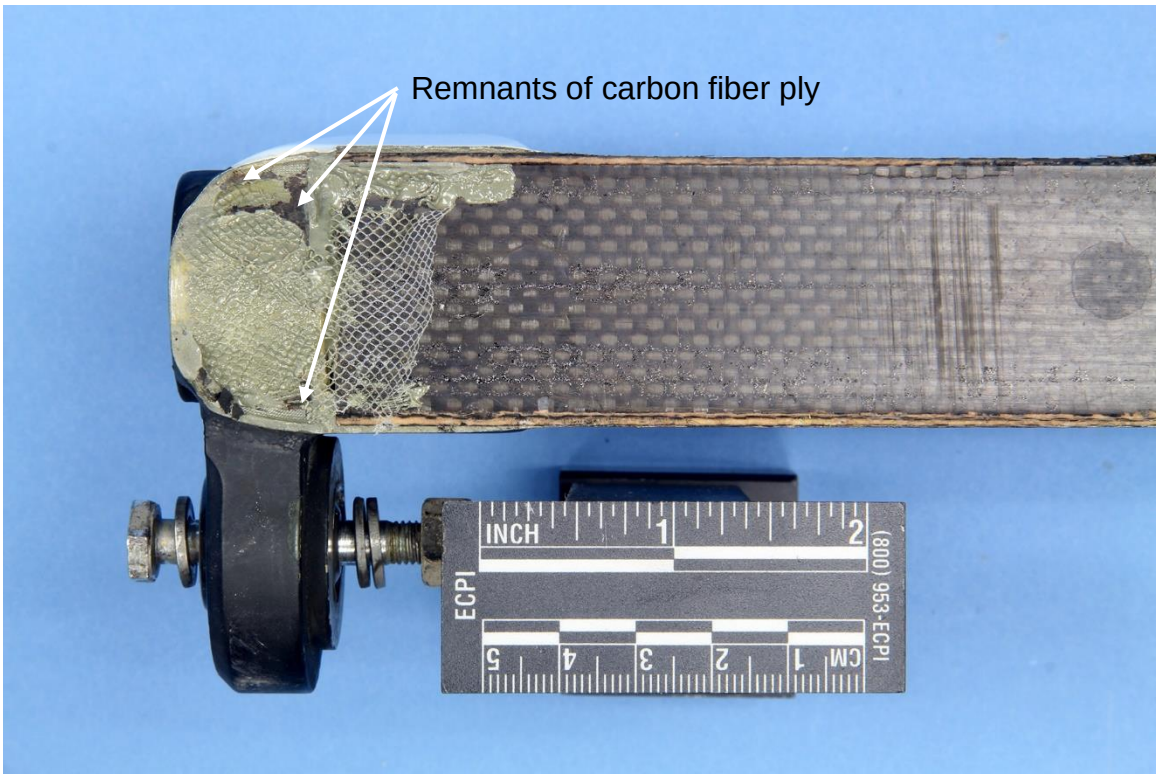

b)

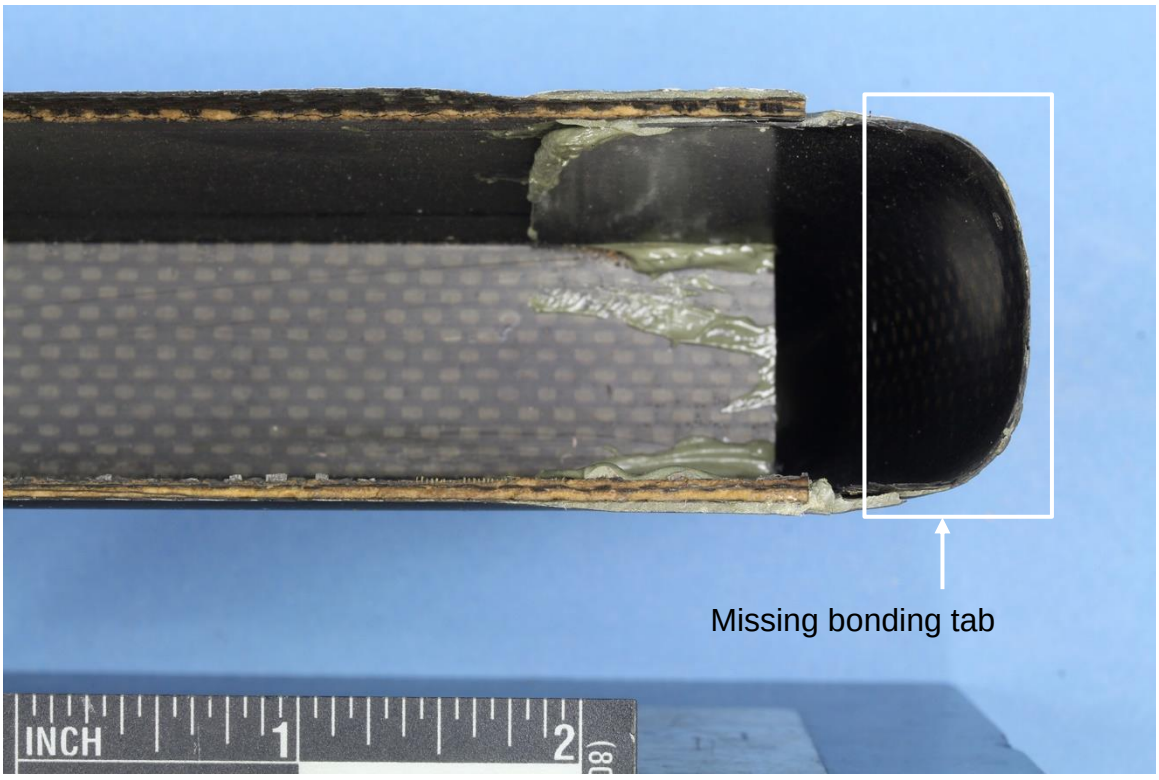

Figure 22. Images of the inboard closeout separation: a) spar side and b) afterbody side. The closeout tab for bonding to the inboard aluminum fitting was missing.

a)

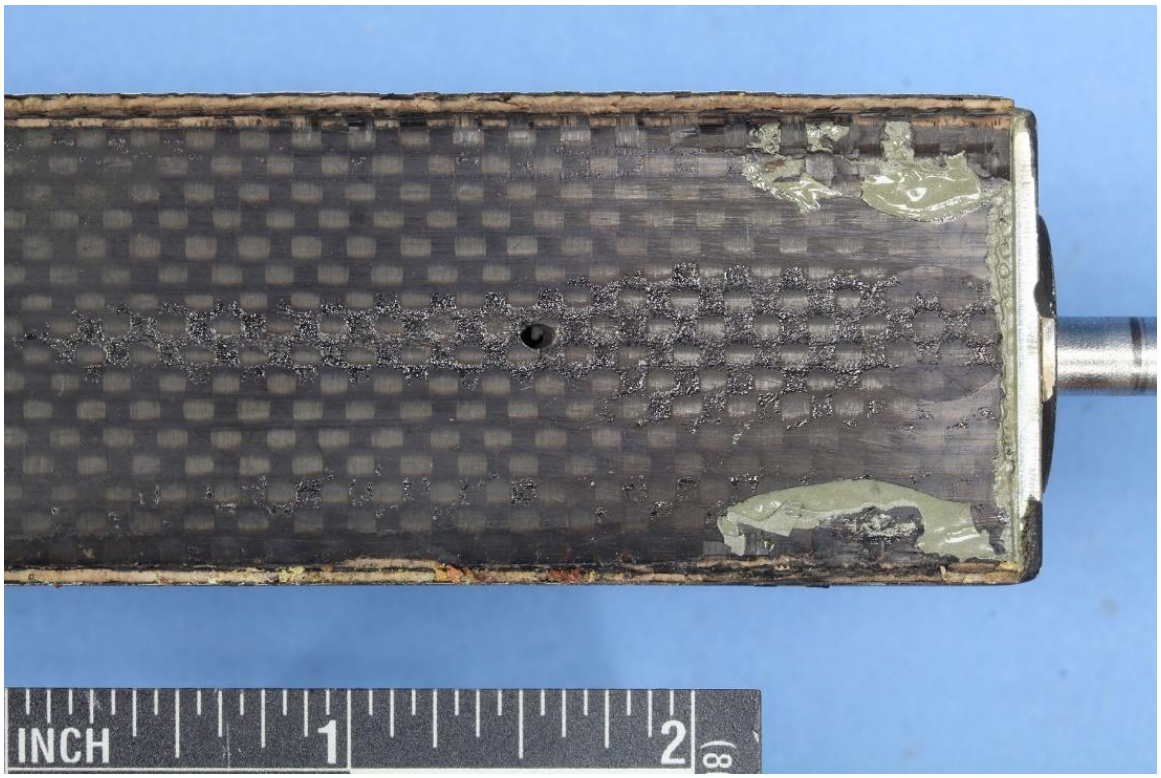

b)

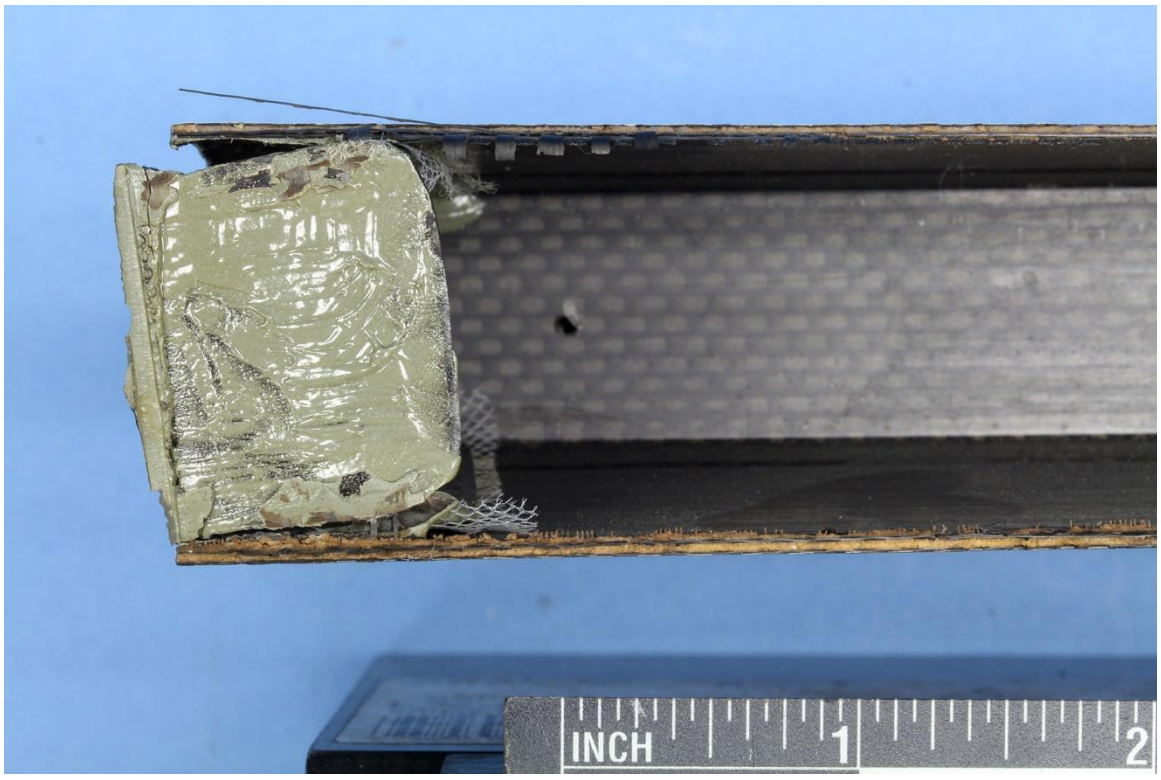

Figure 23. Images of the outboard closeout bonding tab separation: a) spar side and b) afterbody side.

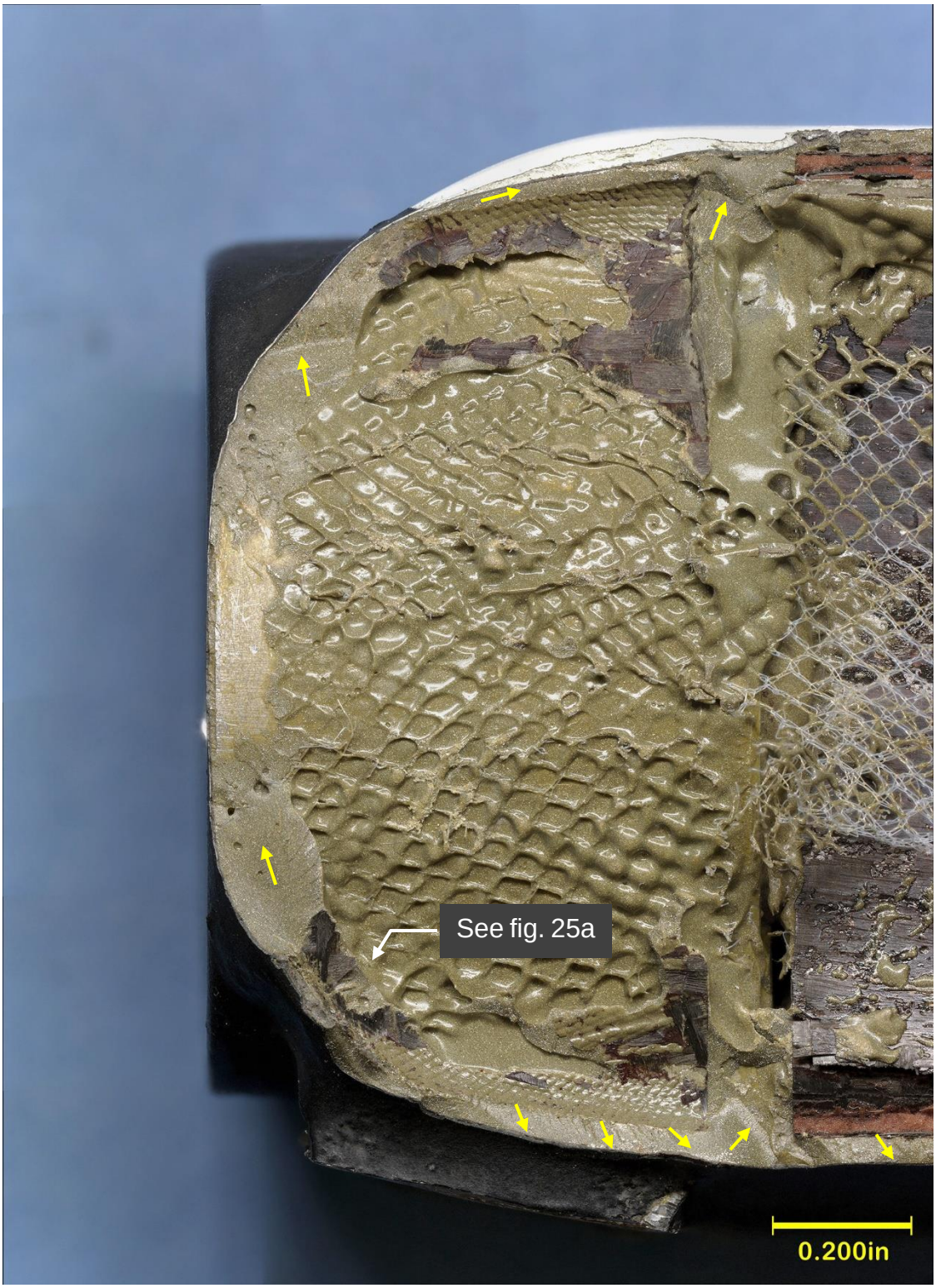

Figure 24. Aft face of the aluminum fitting exhibiting adhesive, scrim cloth, and peel separation of a carbon fiber ply.

a)

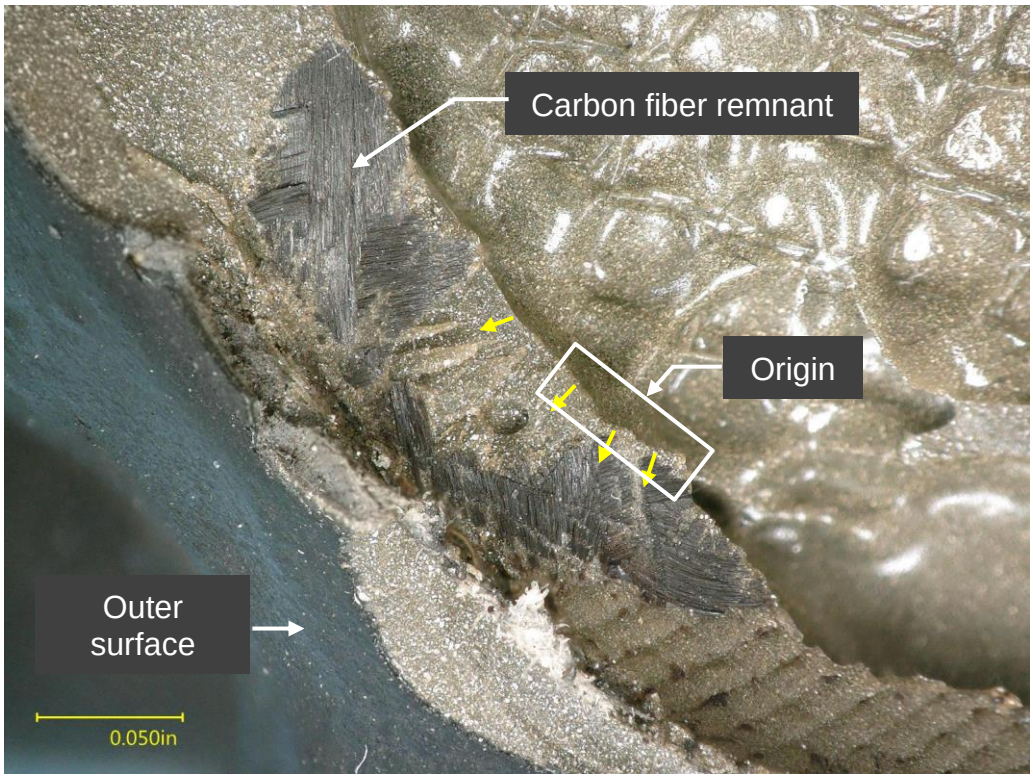

b)

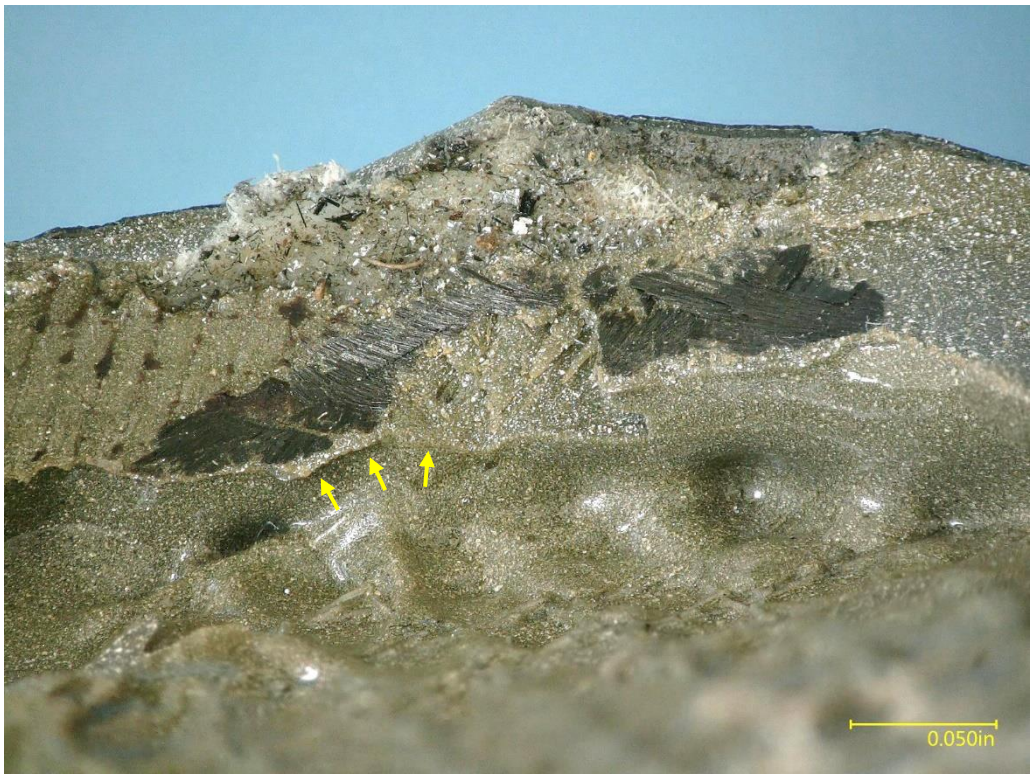

Figure 25. Images of the inboard closeout fracture origin area: a) plan view and b) oblique view.

a)

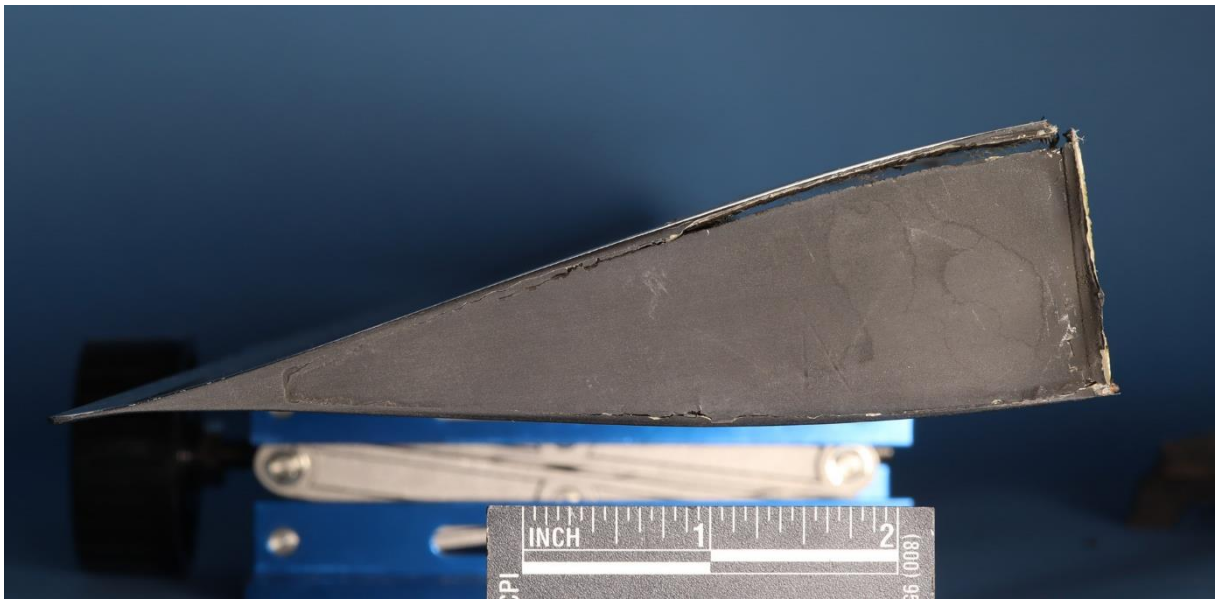

b)

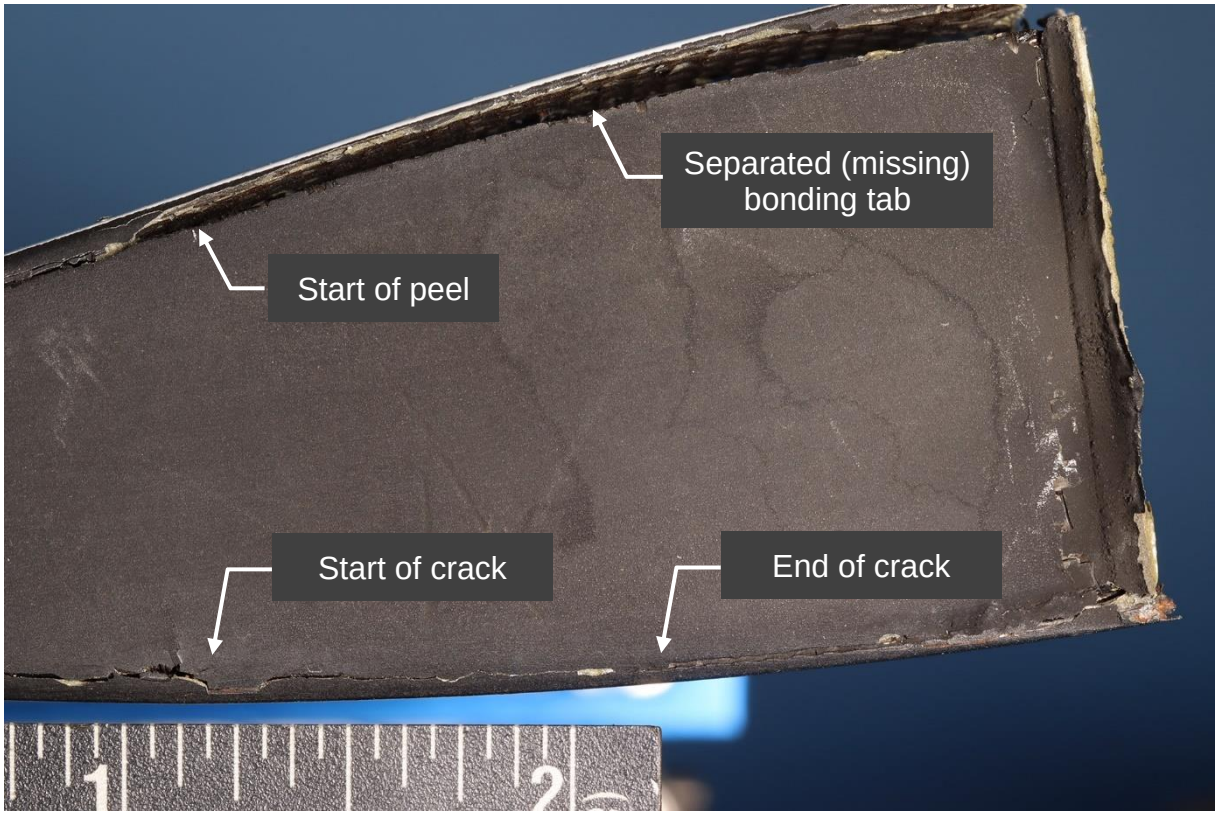

Figure 26. Images of the outboard closeout: a) overview; b) image indicating end of crack along lower edge and peel region of bonding tab along upper edge; and

c)

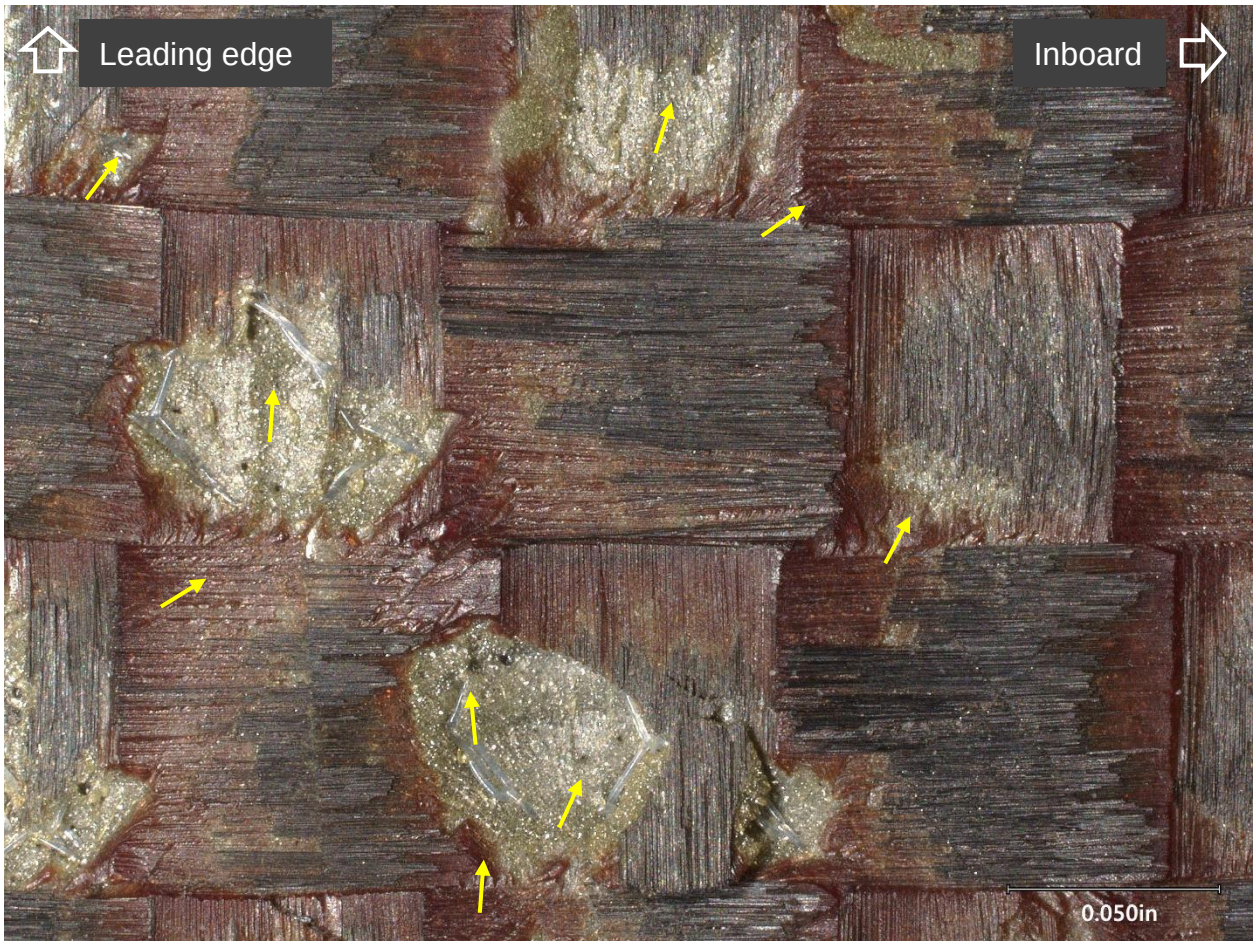

Figure 26 (cont.). c) Upper skin, interior surface at outboard end of the flap where an outboard closeout bonding tab had separated. Local crack propagation marks in the adhesive and resin, indicated by yellow arrows, point toward the leading edge and the inboard direction.

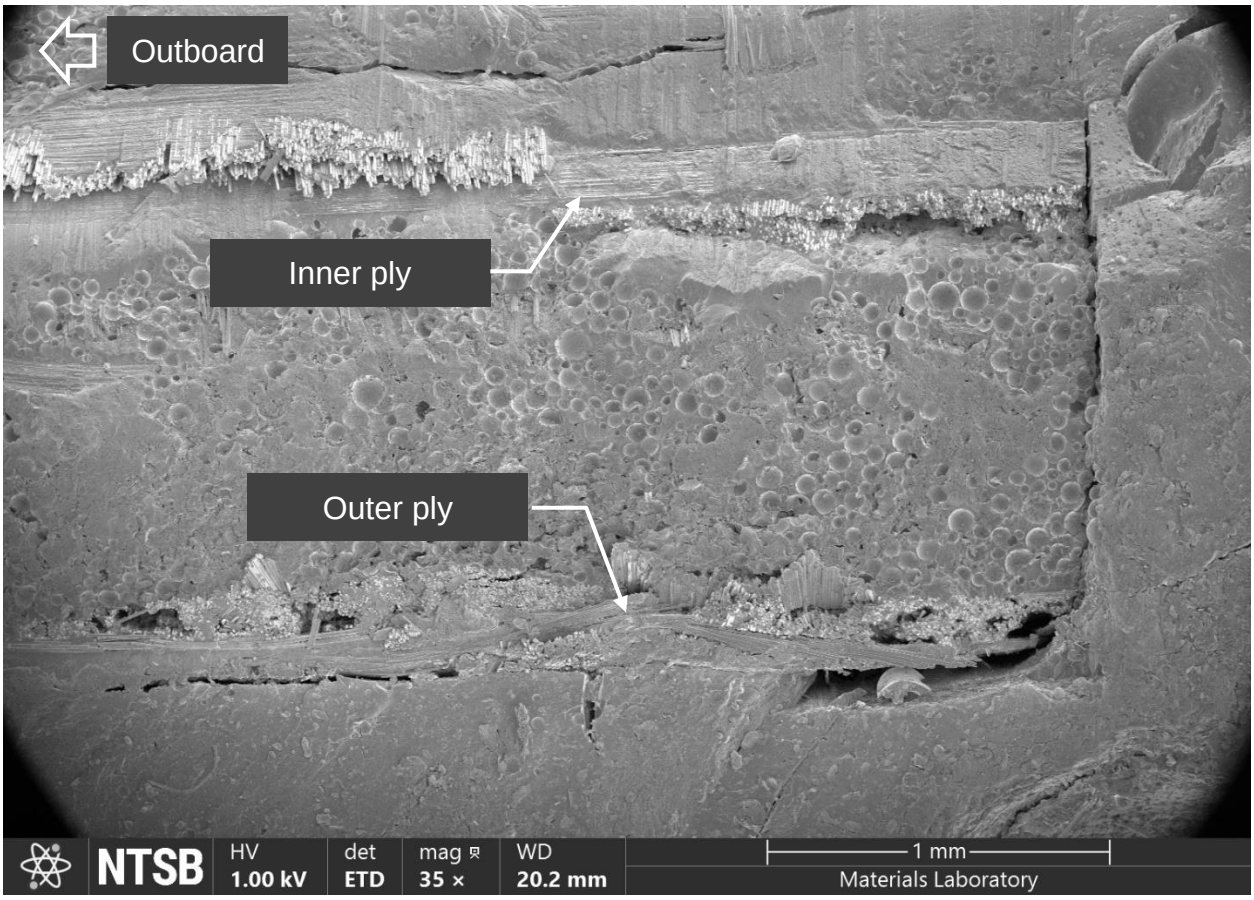

Figure 27. SEM image of the servo flap afterbody fracture: afterbody side, lower surface, inboard end. The view is toward the trailing edge.

a)

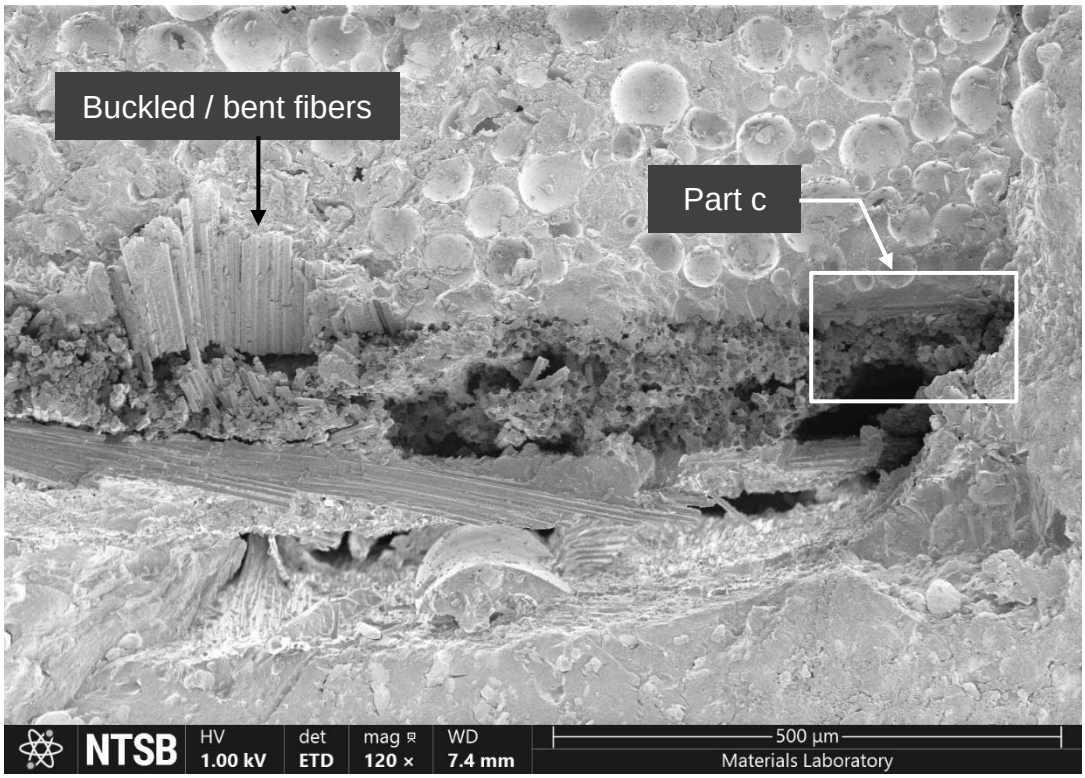

b)

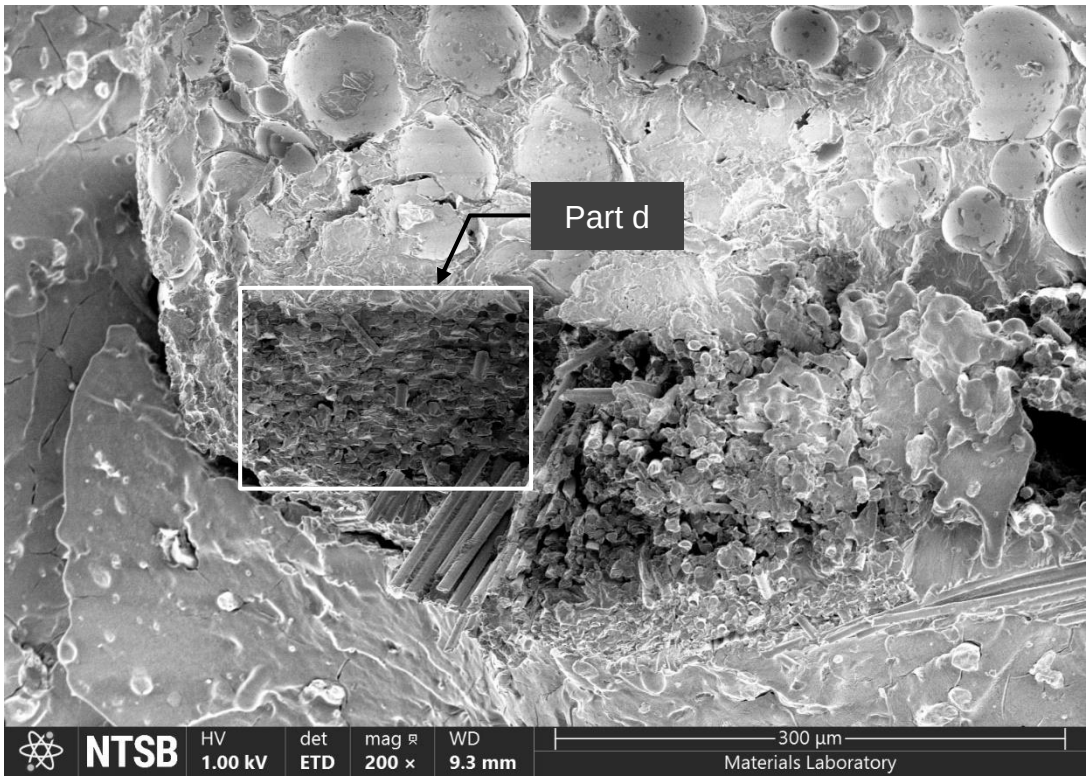

Figure 28. SEM images of the spar / afterbody fracture at the lower surface, inboard end, outer ply: a) afterbody-side of fracture; b) spar-side of fracture;

c)

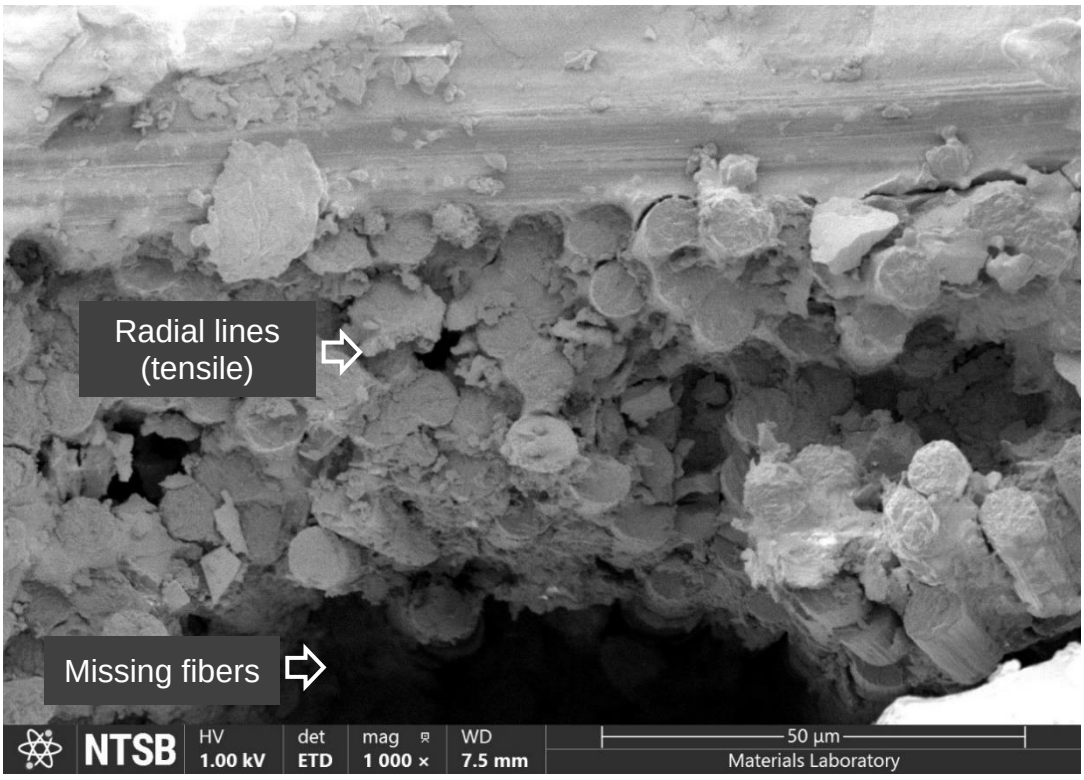

d)

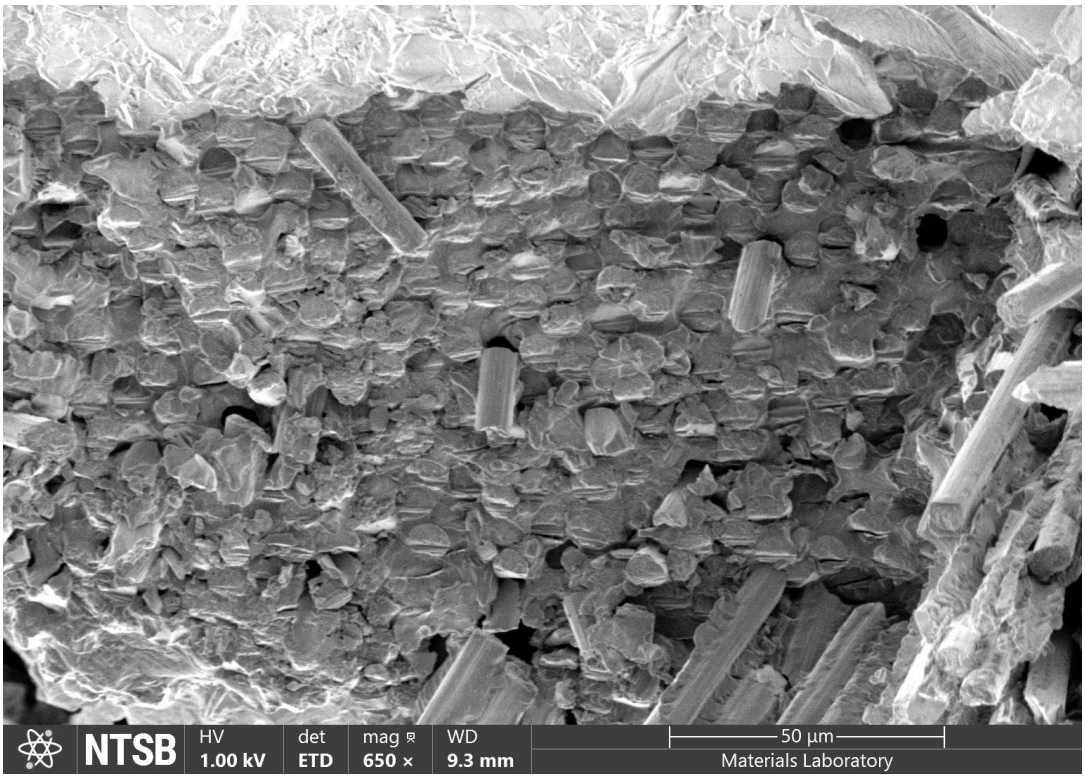

Figure 28 (cont.). c) higher magnification image from part a exhibiting tensile fracture and missing fibers; and d) higher magnification image from b with fibers exhibiting chop marks in a downward bending orientation.

a)

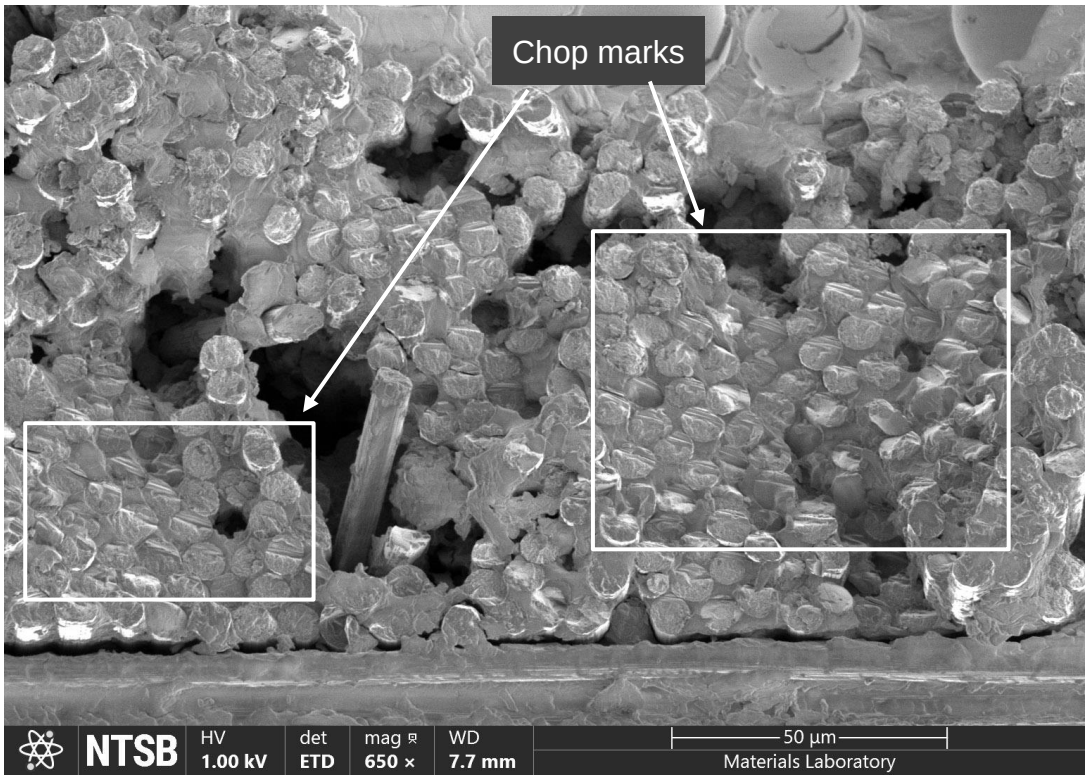

b)

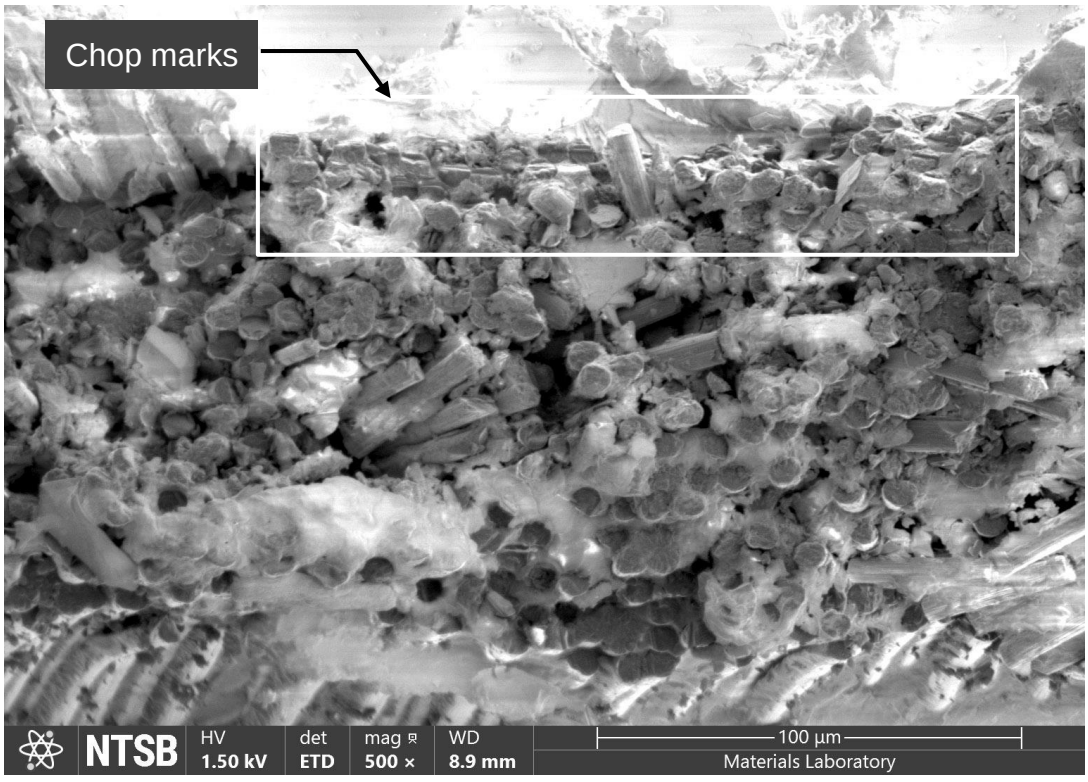

Figure 29. SEM images along skin plies showing chop marks, radial lines, fiber fragments, and debris: a) lower skin, outer ply, spar side, STA 2.00; b) lower skin, inner ply, afterbody-side, STA 6.00; and

c) 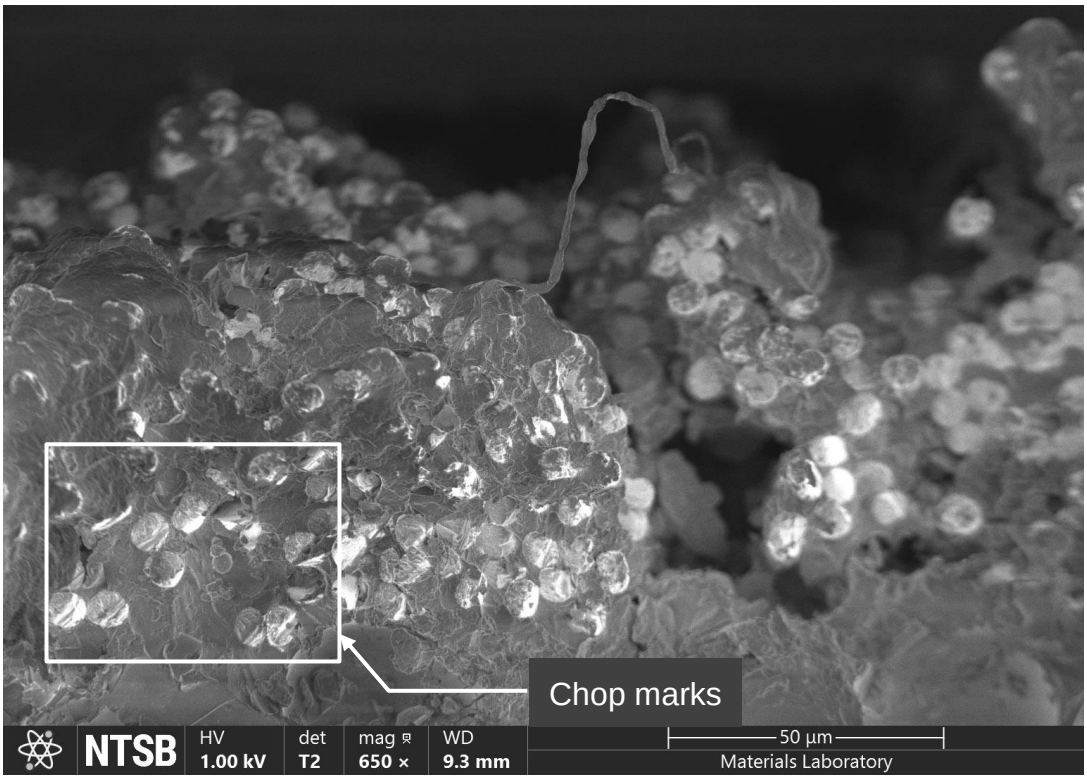

Figure 29 (cont.). c) upper skin, outer ply, afterbody-side, STA 6.04, outboard of upper skin peel region.

a)

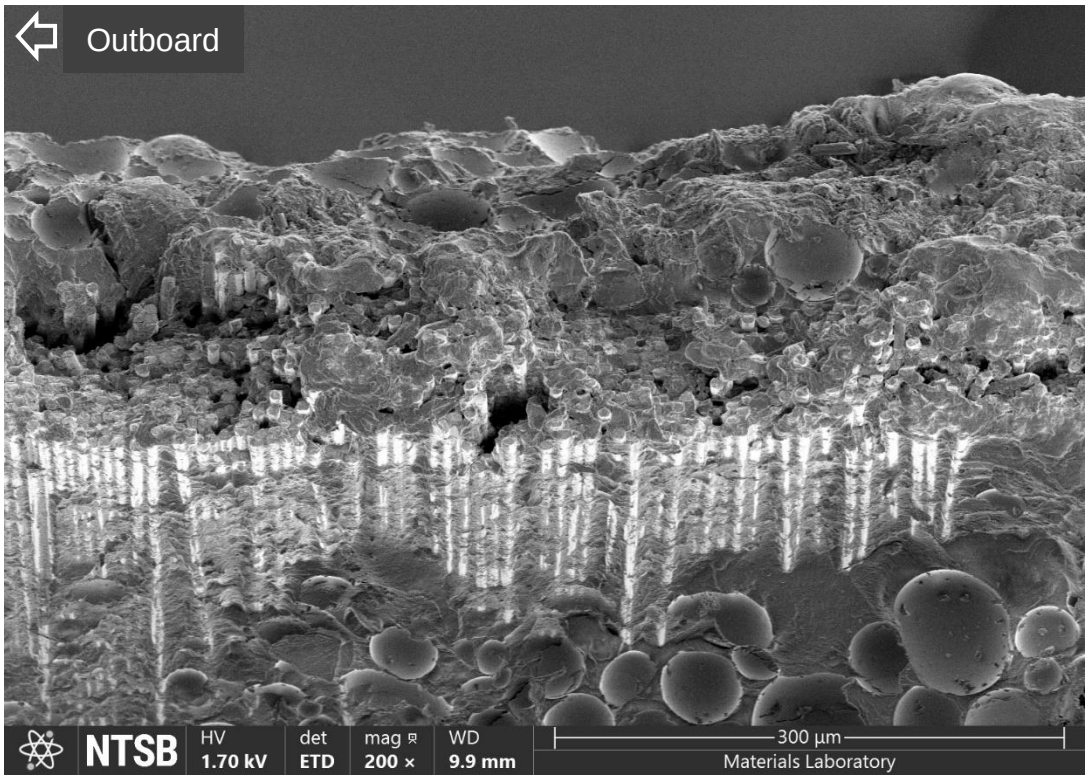

b)

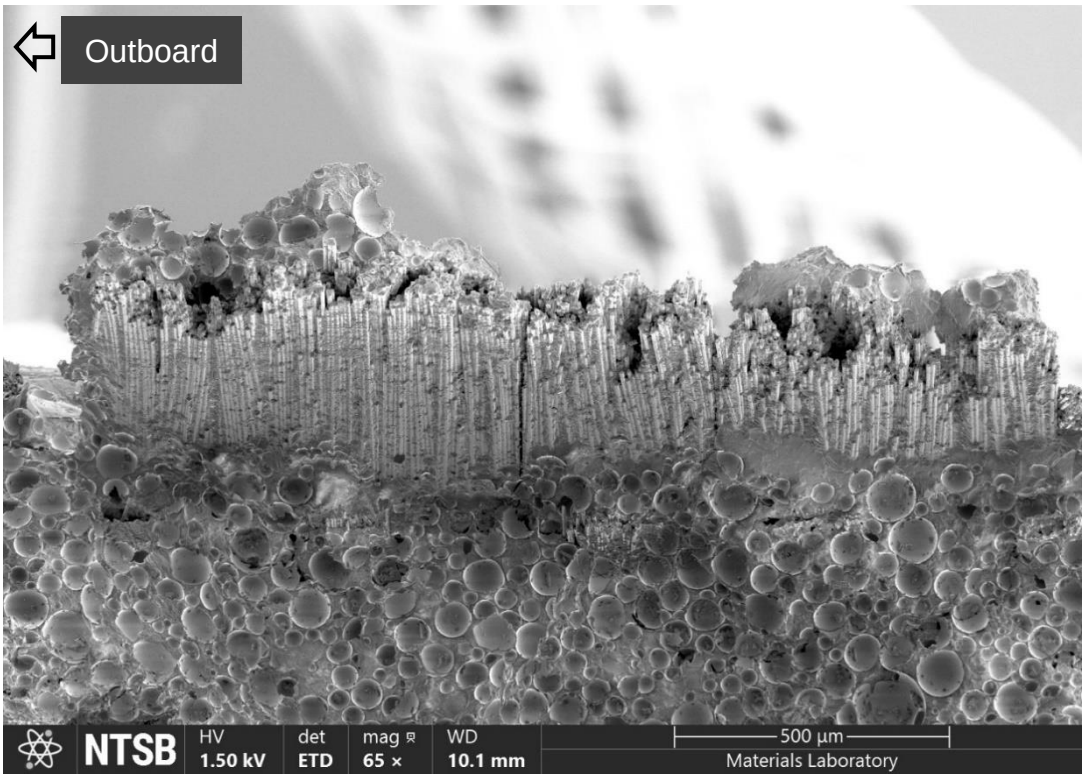

Figure 30. SEM images of fractured lower skin inner ply tows: a) peel along fiber tow at approximately STA 17.24 and b) peel along fiber tow at approximately STA 27.98.

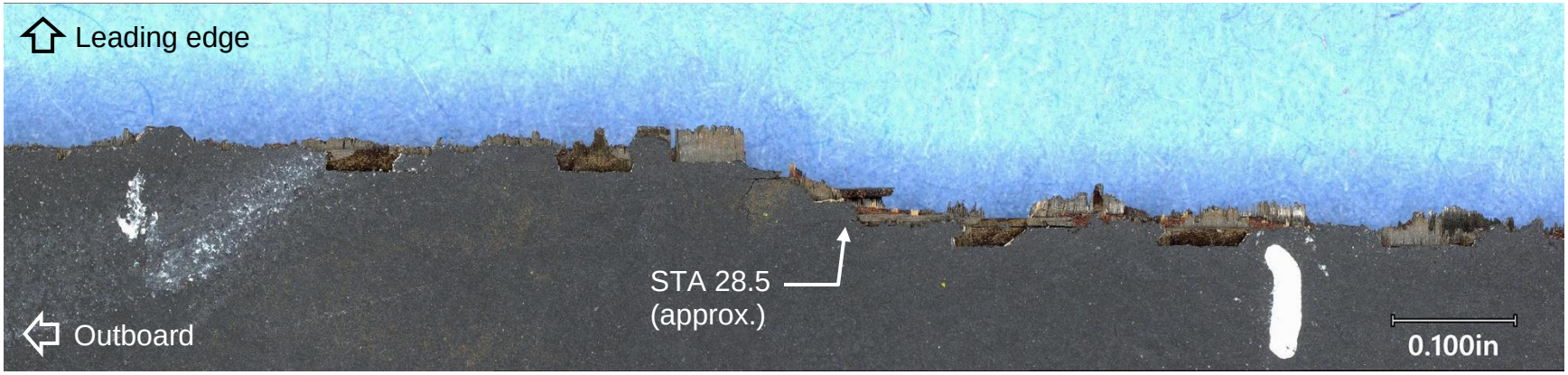

Figure 31. Image of servo flap lower afterbody skin showing chordwise (toward leading edge) shift in fracture path at approximately STA 28.5.

a)

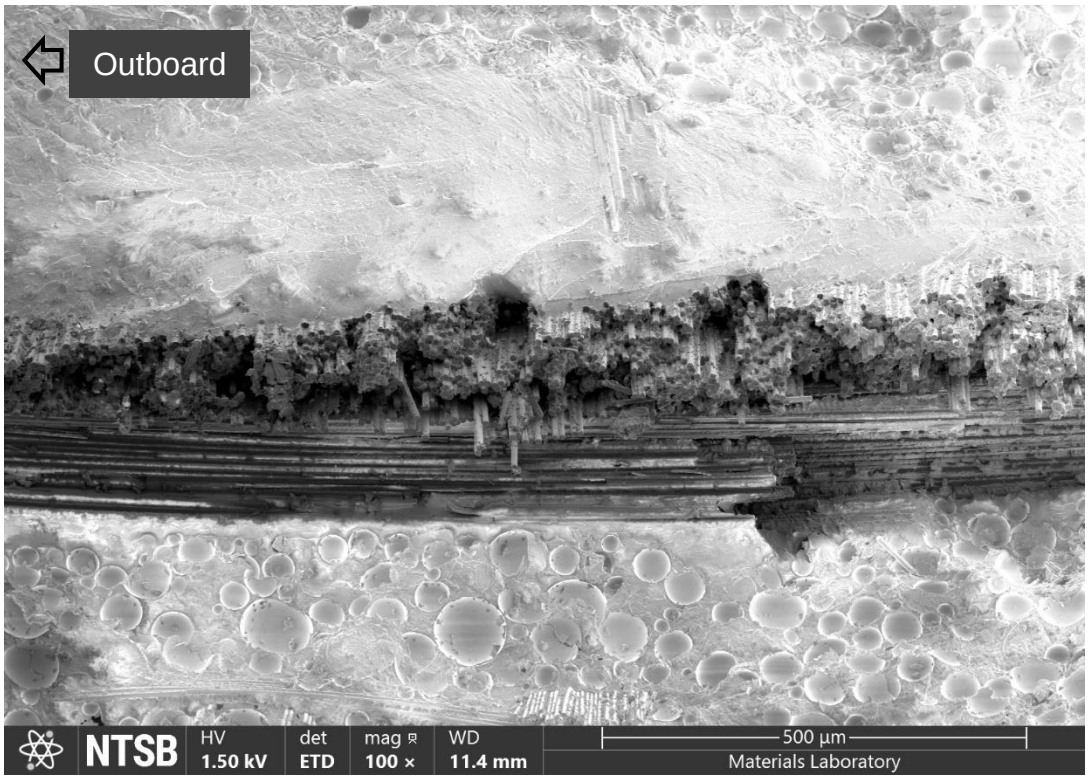

b)

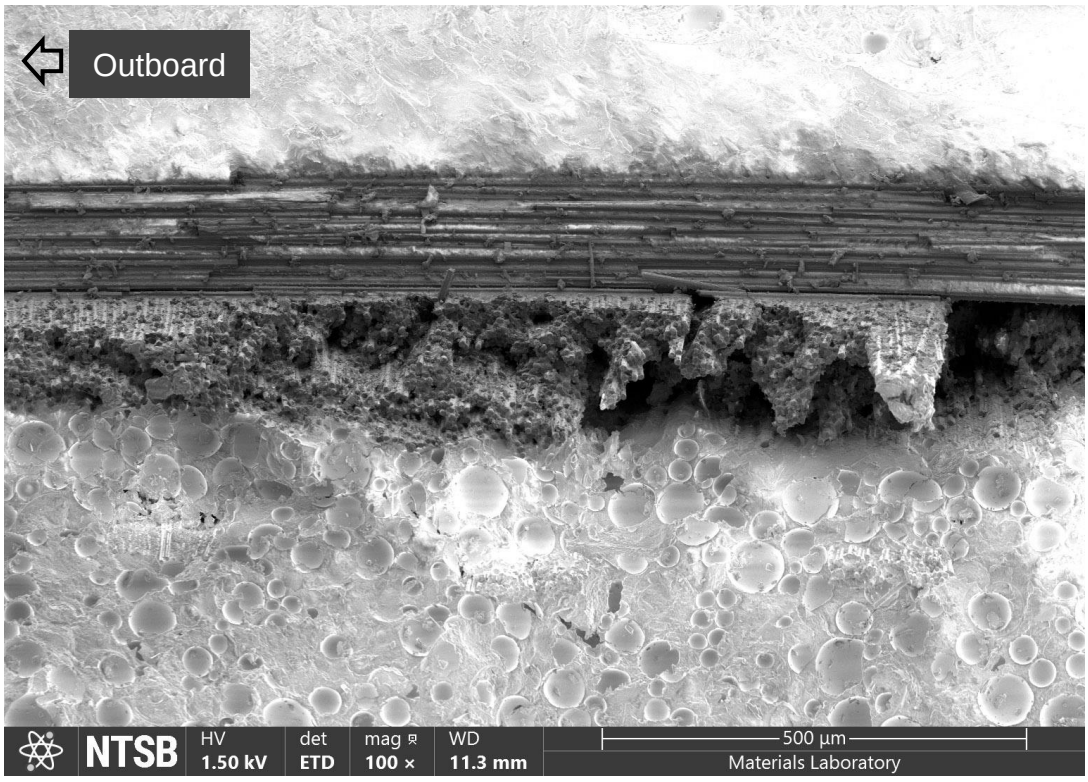

Figure 32. SEM images of fractured lower skin inner ply tows: a) transverse fracture at approximately STA 28.80 and b) transverse fracture at approximately STA 28.88.

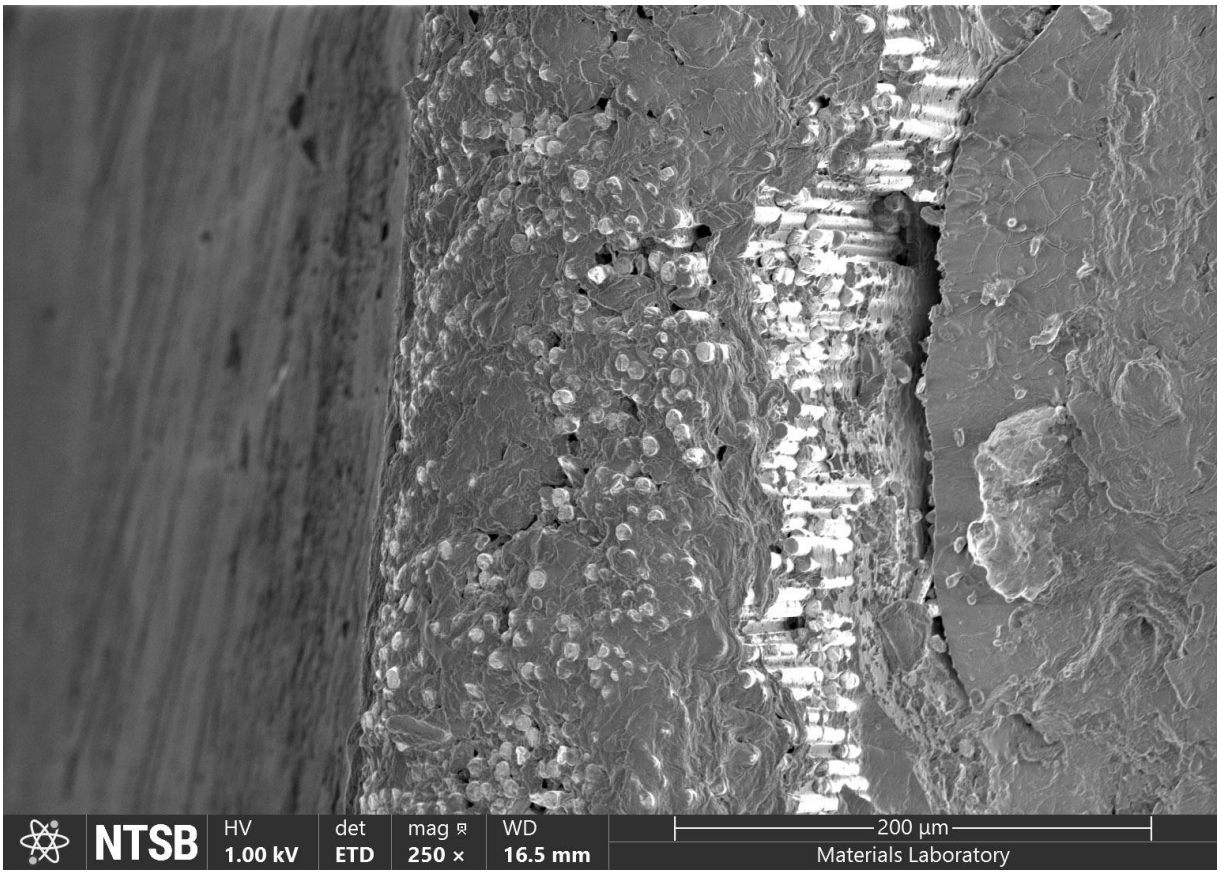

Figure 33. Fractured carbon fiber ply where the bonding tab separated from the body of the inboard closeout, showing rubbing and debris.

a)

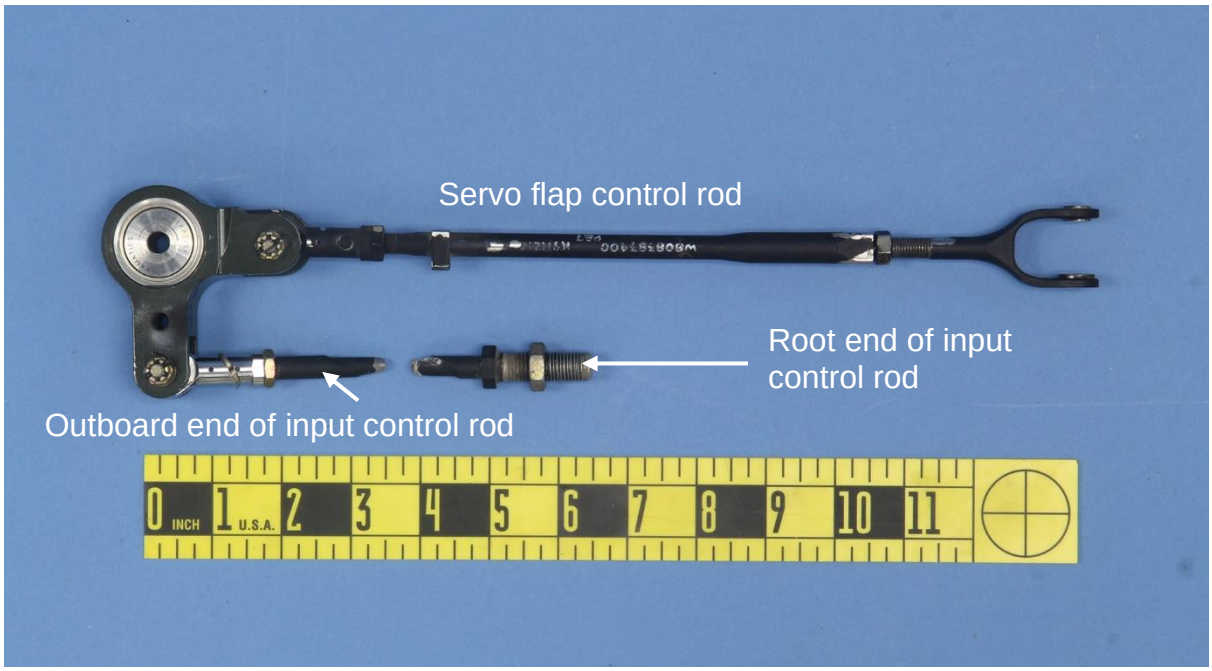

b)

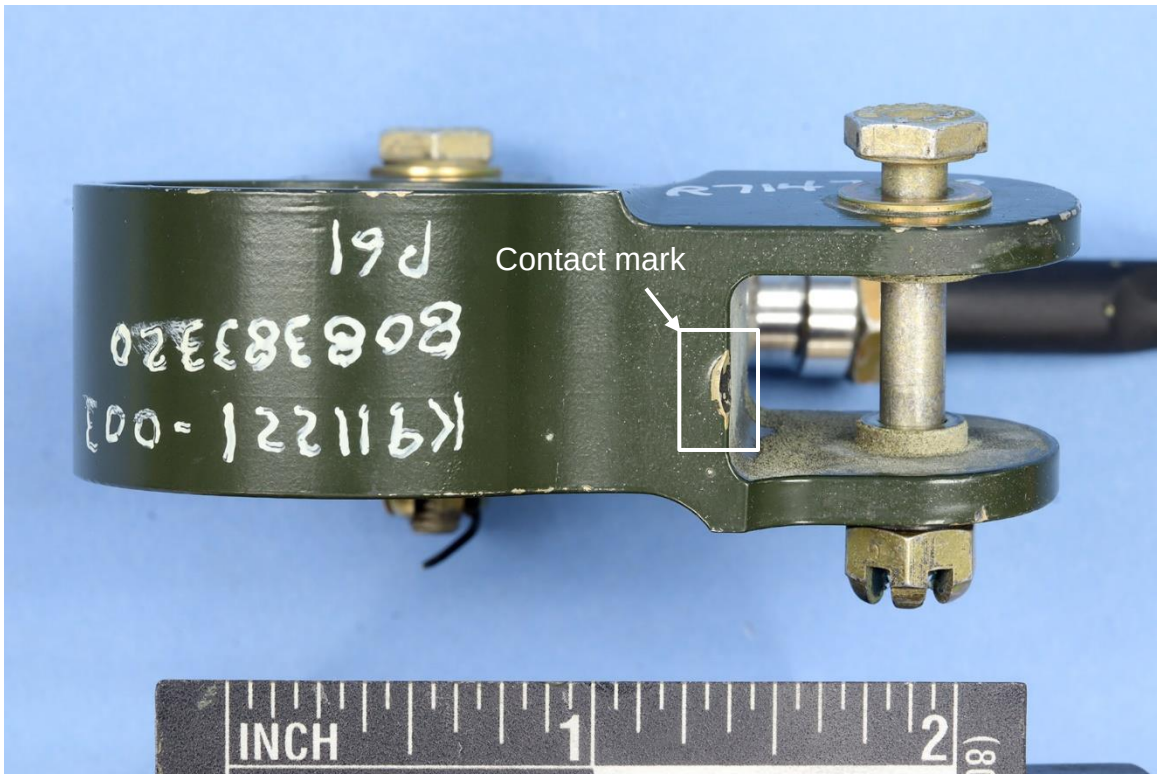

Figure 34. a) LHW servo flap control rod, bellcrank, and fractured input control rod (located internal to MRB) and b) contact mark on bellcrank.

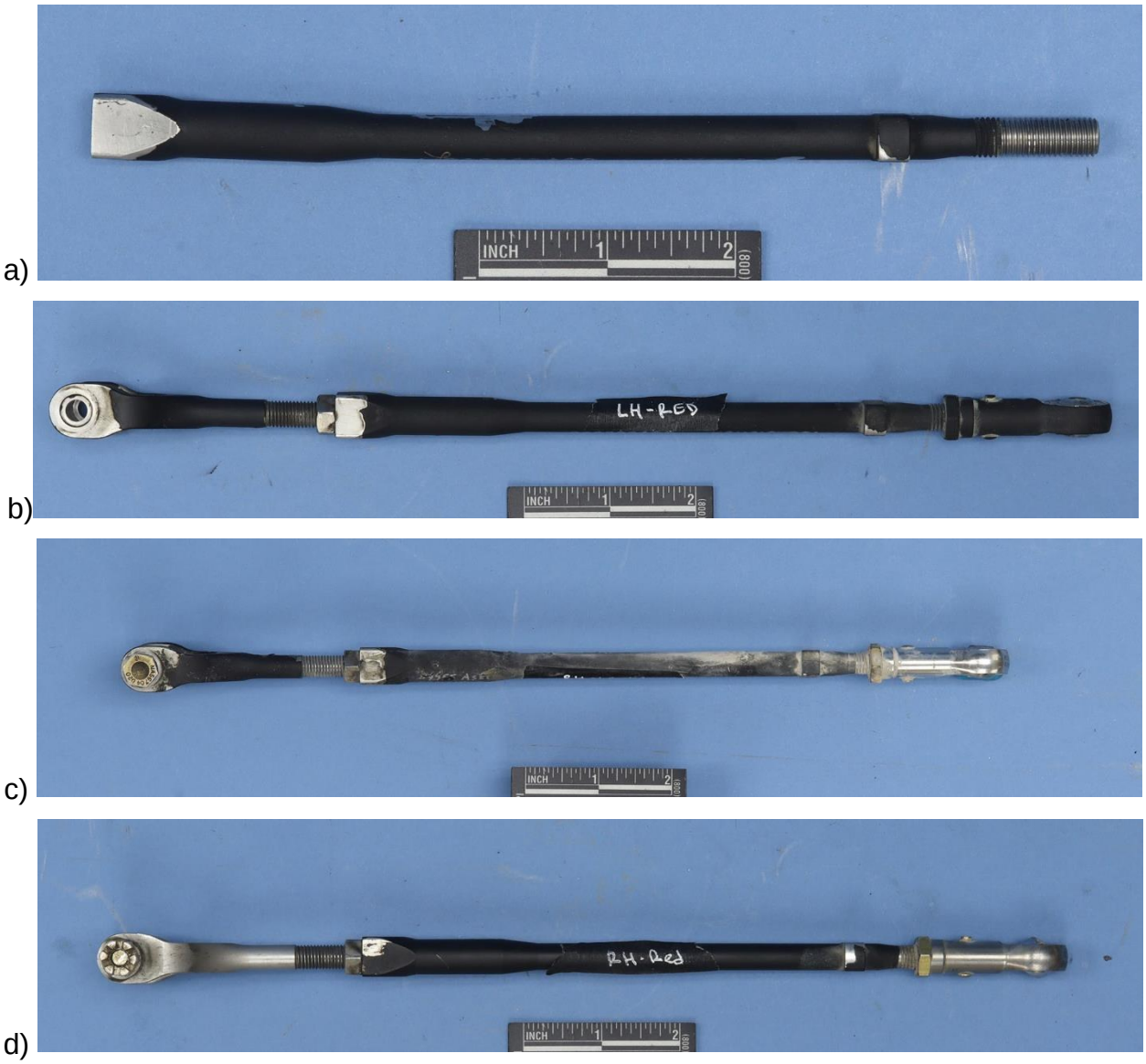

Figure 35. Servo flap control rods: a) LHW; b) LHR; c) RHW; and d) RHR.

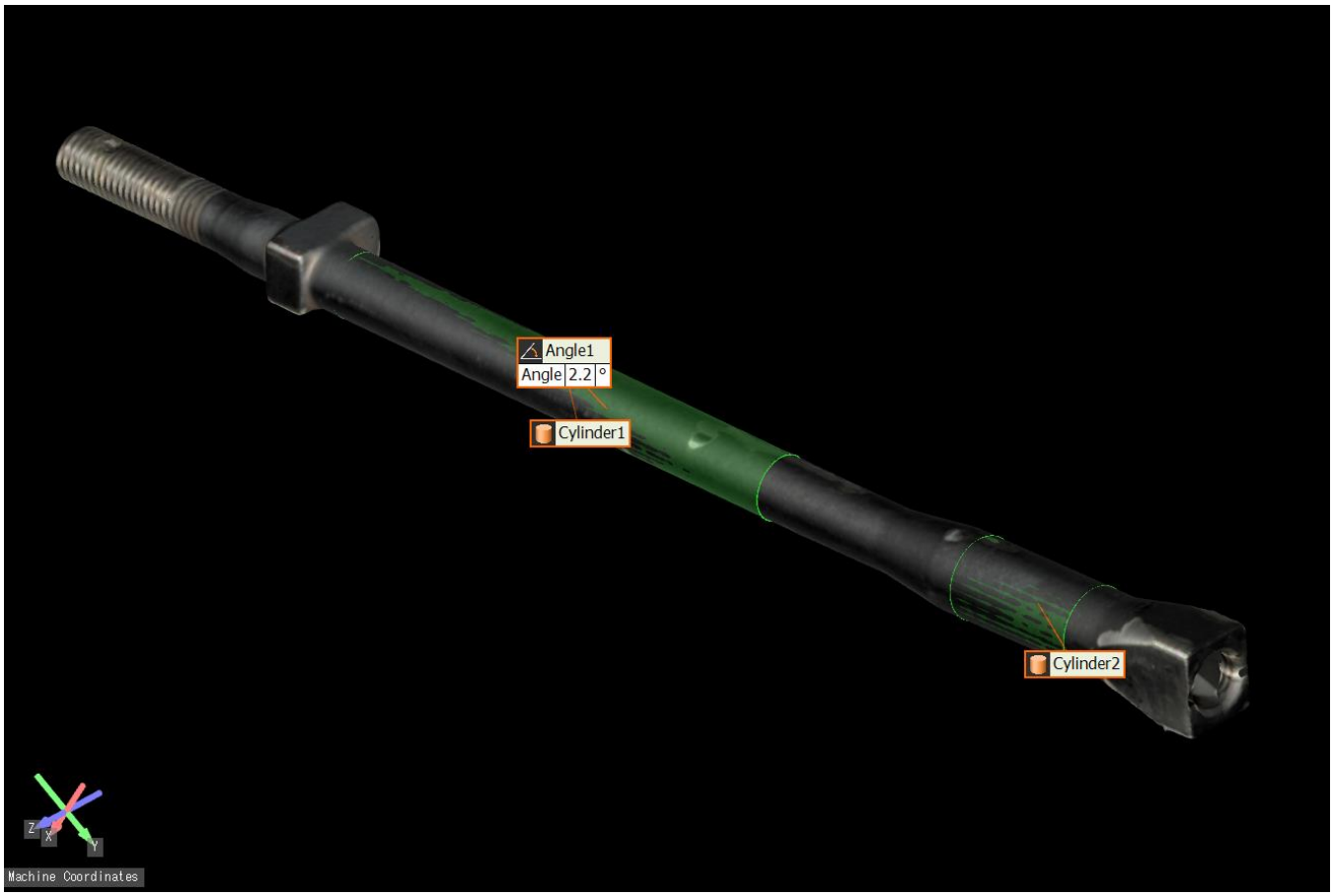

Figure 36. 3D structured light scan of LHW control rod. The image shows the objects used to measure the bend angle and the result.

a)

b)

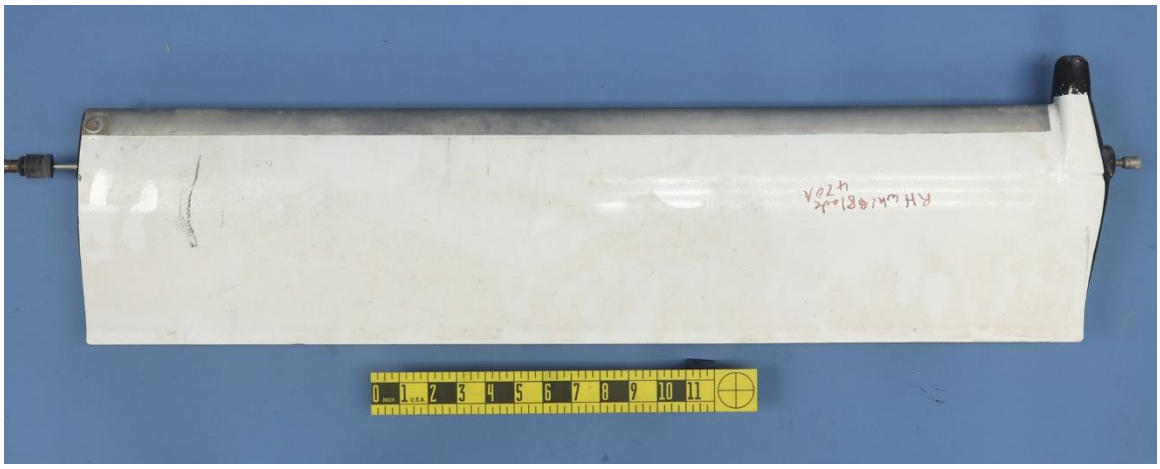

c)

Figure 37. Sister flaps from the accident aircraft: a) LHR; b) RHW; and c) RHR

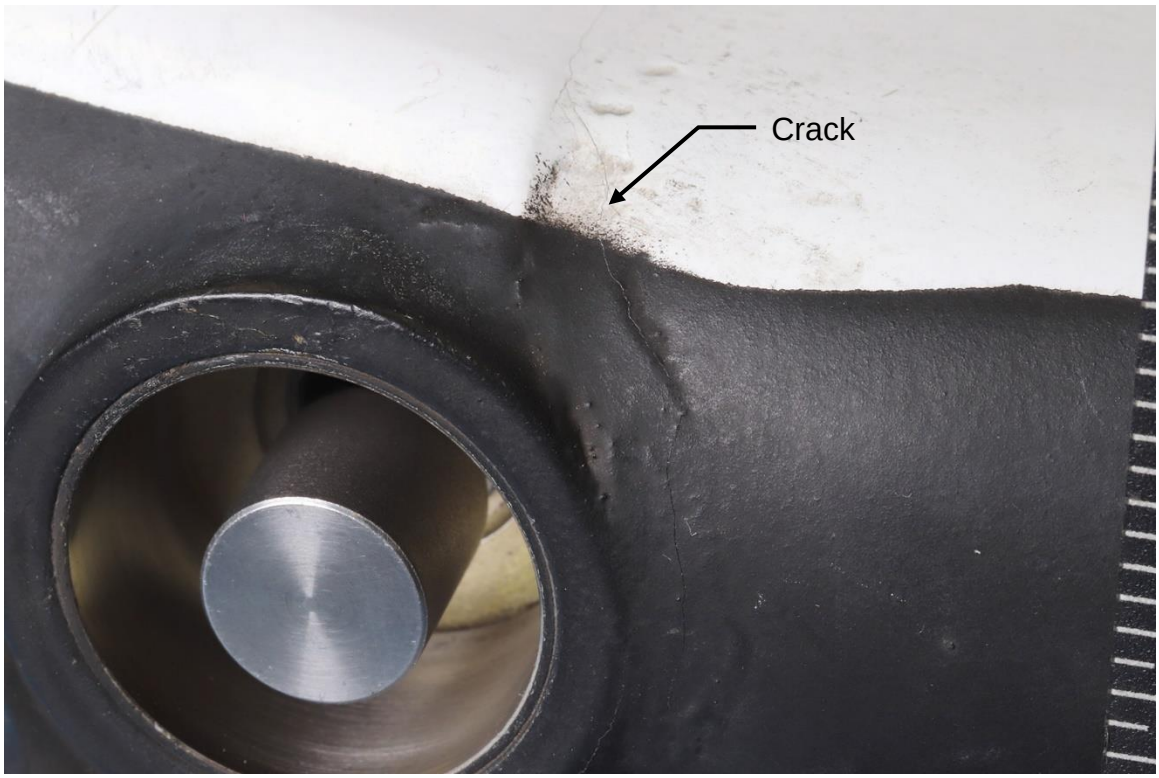

Figure 38. Hairline crack along upper side of inboard closeout on the LHR servo flap.

a)

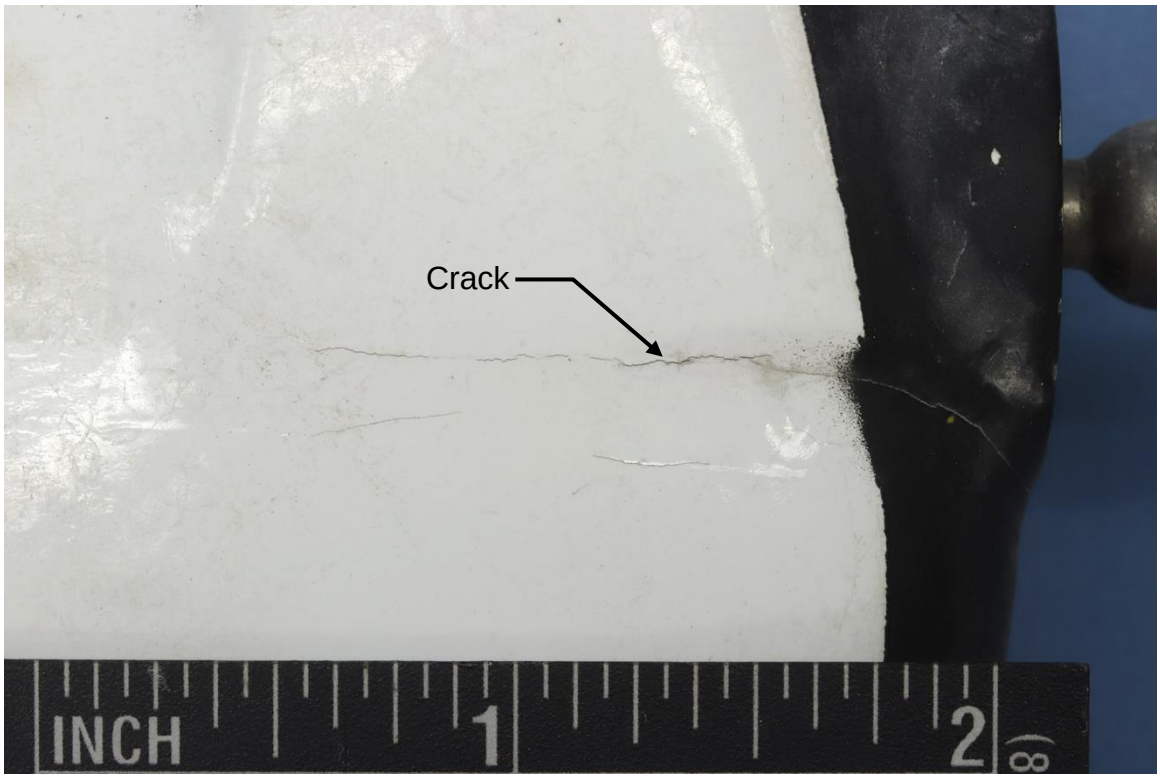

b)

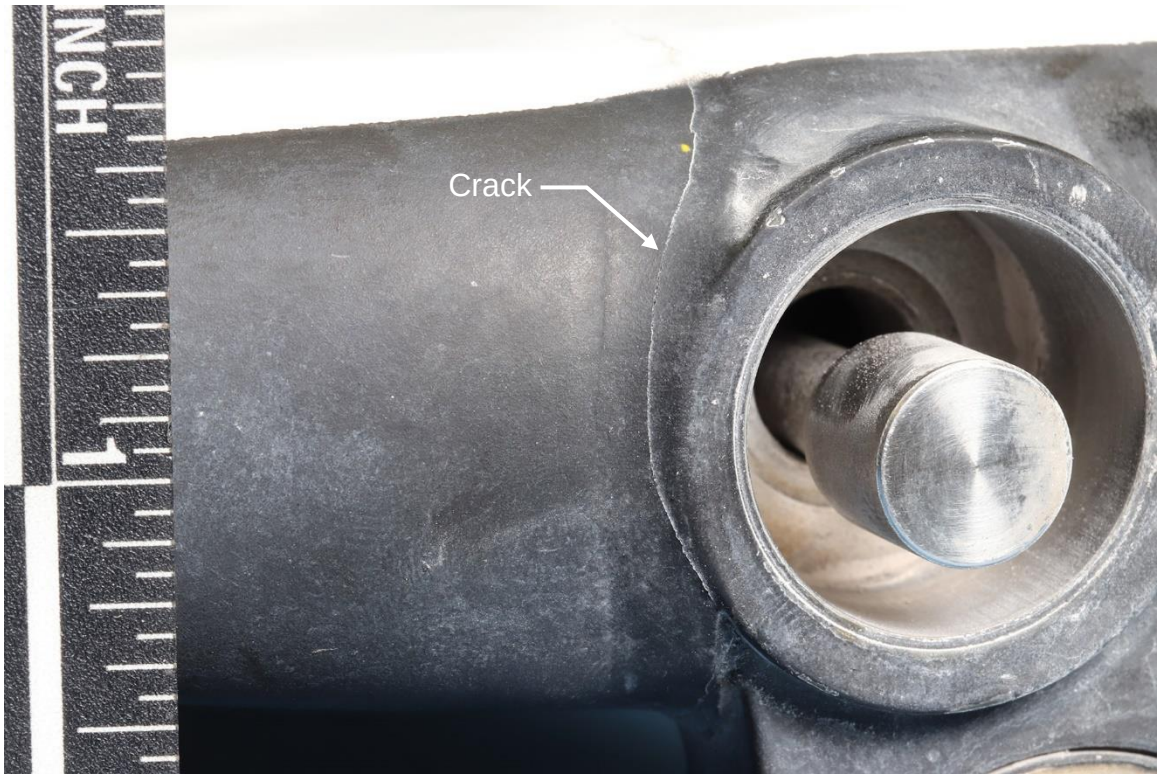

Figure 39. Images of cracks along edge of inboard closeout bond line on RHW servo flap: a) top side of closeout; b) inboard side of closeout; and

c) 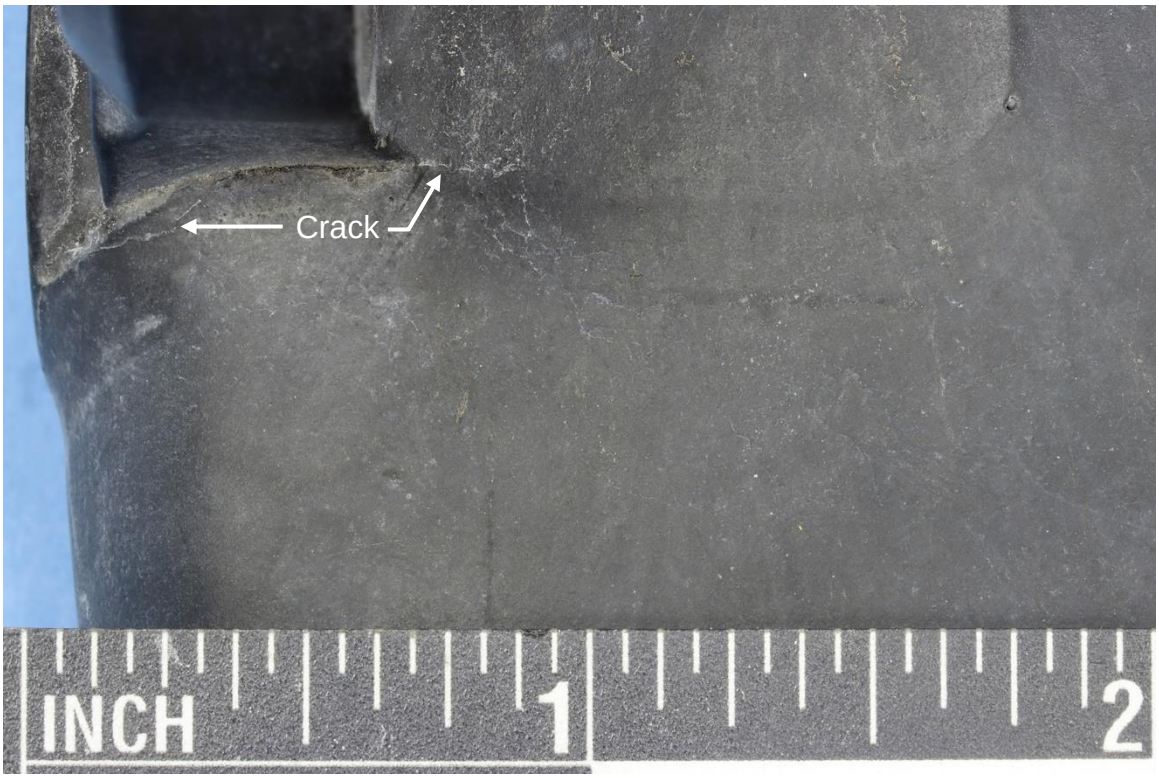

Figure 37 (cont.). c) lower side of closeout.

a)

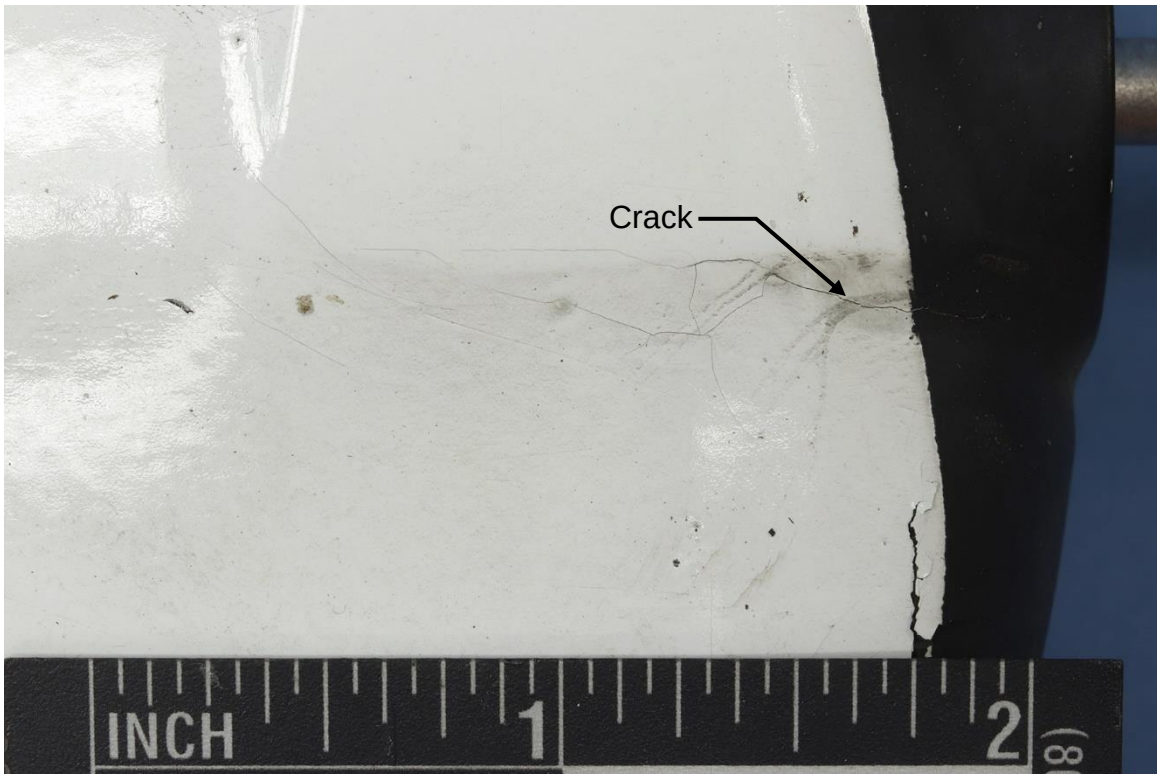

b)

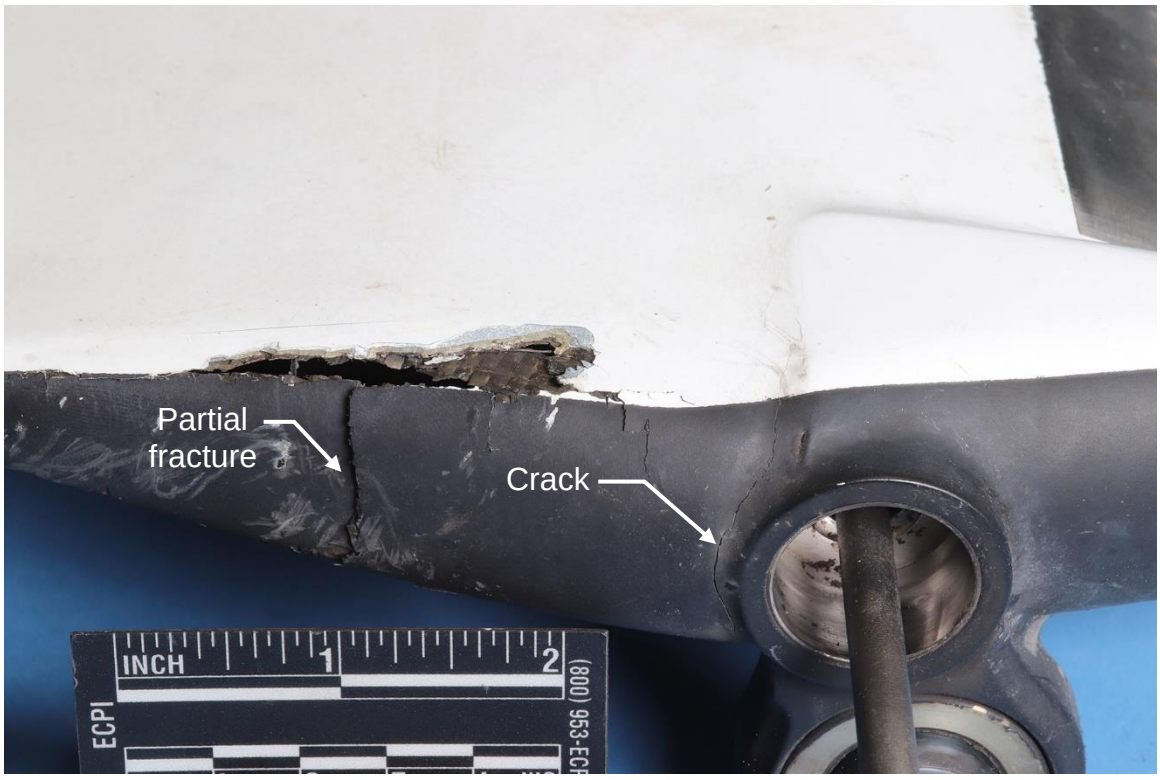

Figure 40. Images of cracks along edge of inboard closeout bond line on RHR servo flap: a) top side of closeout; b) inboard side of closeout;

c)

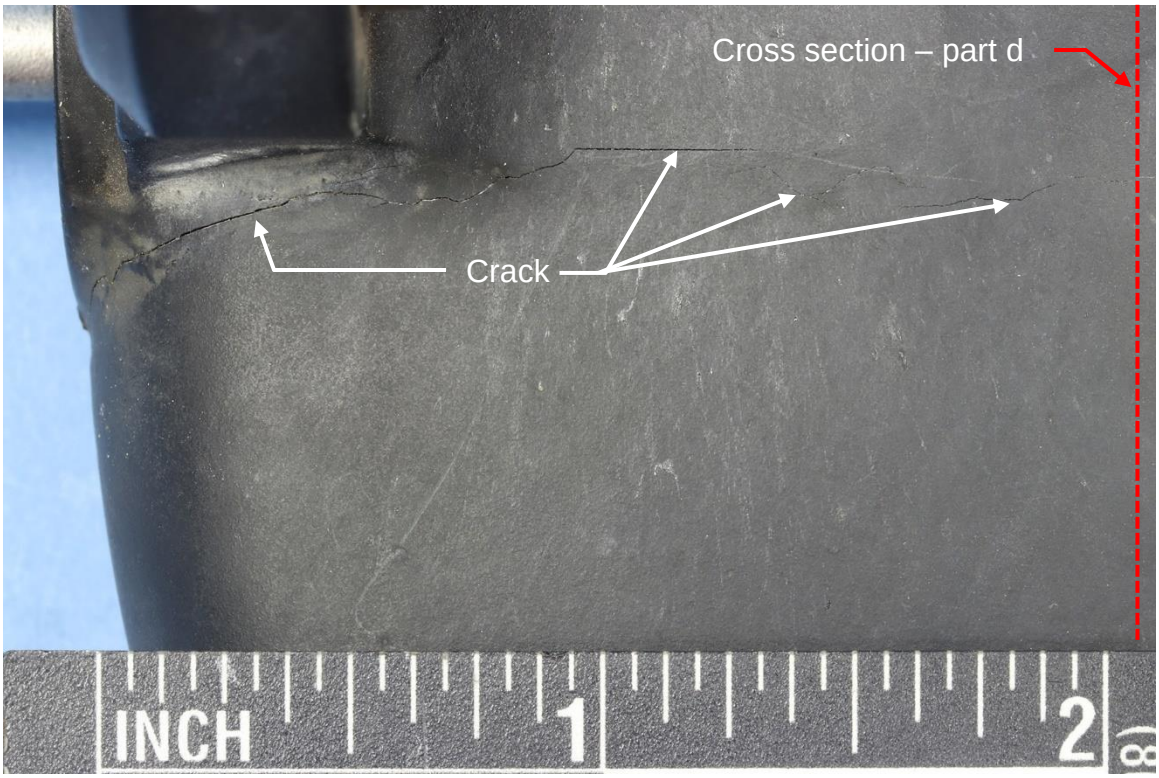

d)

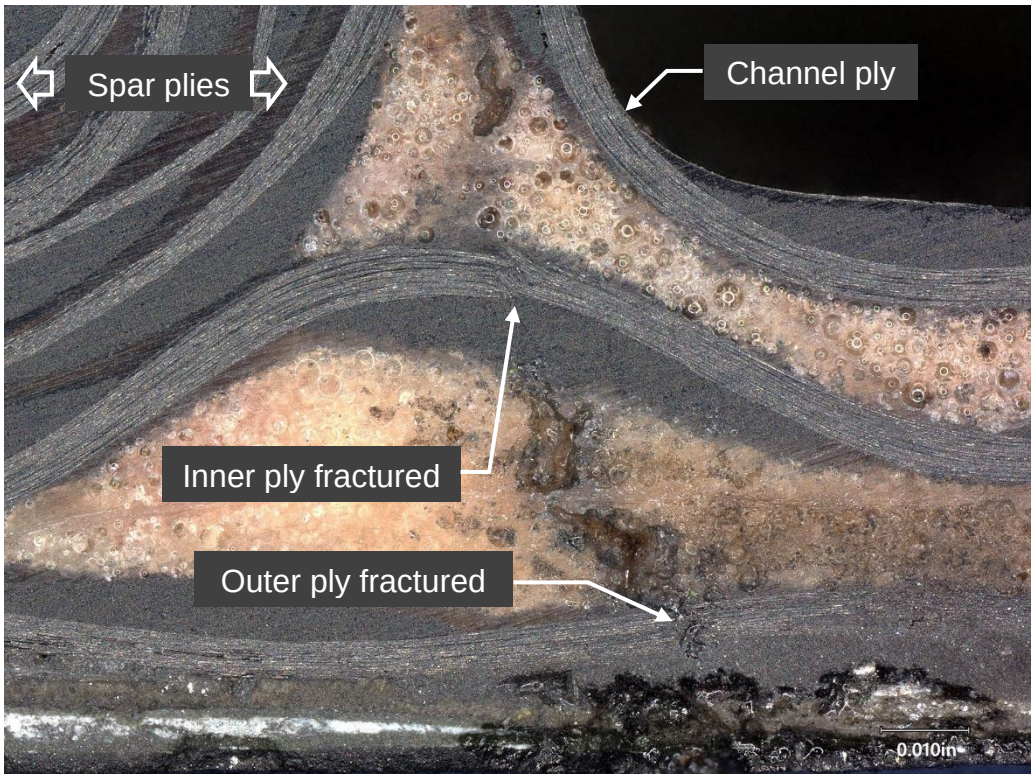

Figure 38 (cont.). c) lower side of closeout; and d) cross section through lower skin plies at location indicated in part c. The surface crack extended through the outer ply and inner ply.

a)

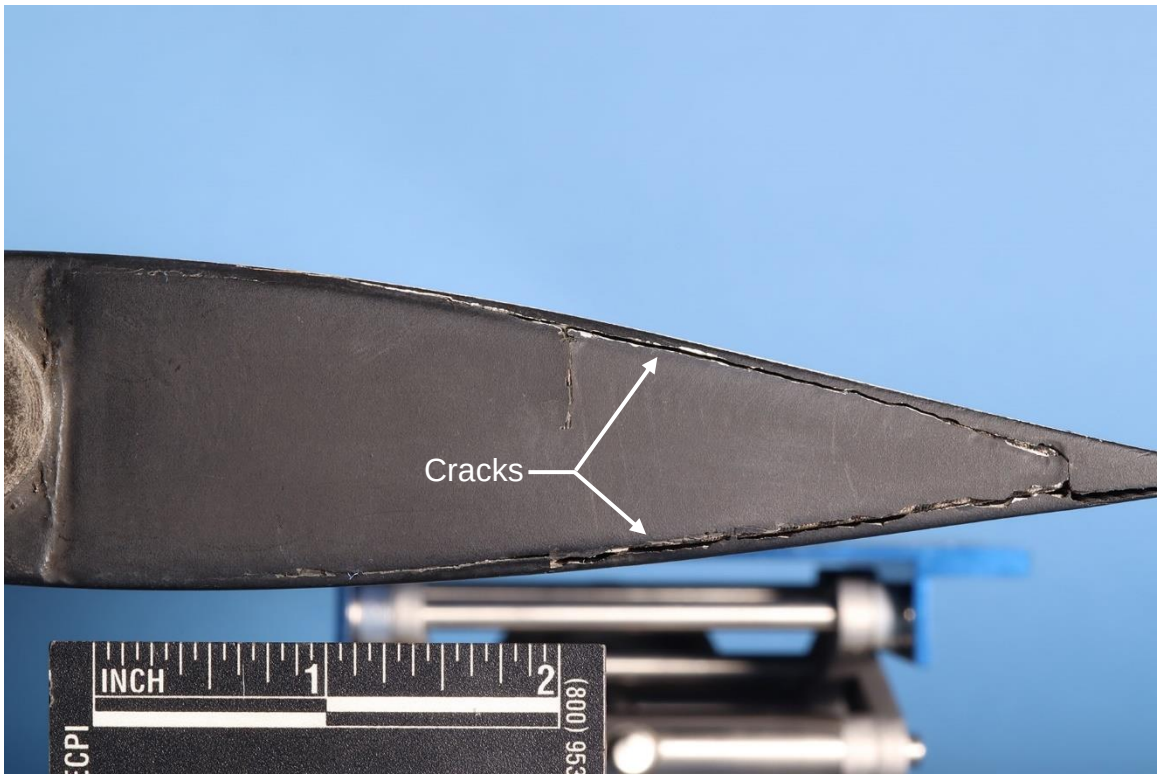

b)

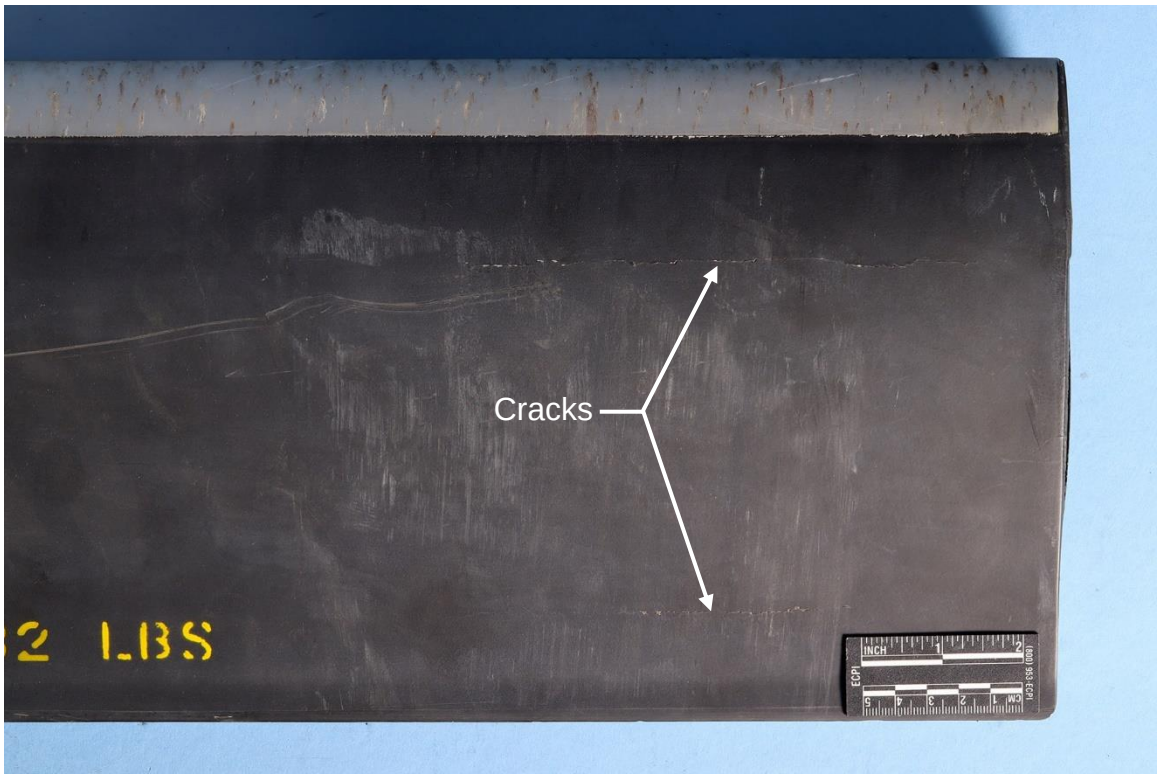

Figure 41. Images of RHR servo flap: a) cracks along upper and lower edges of outboard closeout and b) spanwise cracks along outboard end of lower surface. One crack was at or near the aft end of the D-spar and the other was at or near the forward end of the trailing edge.

a)

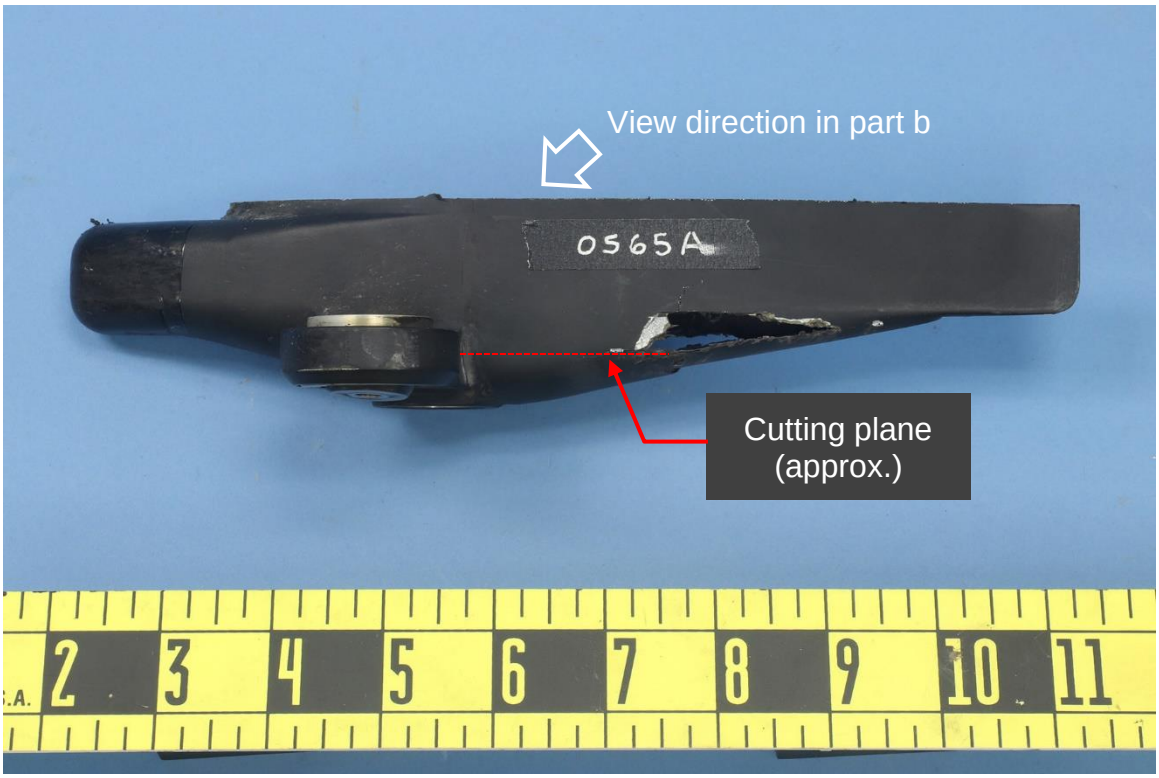

b)

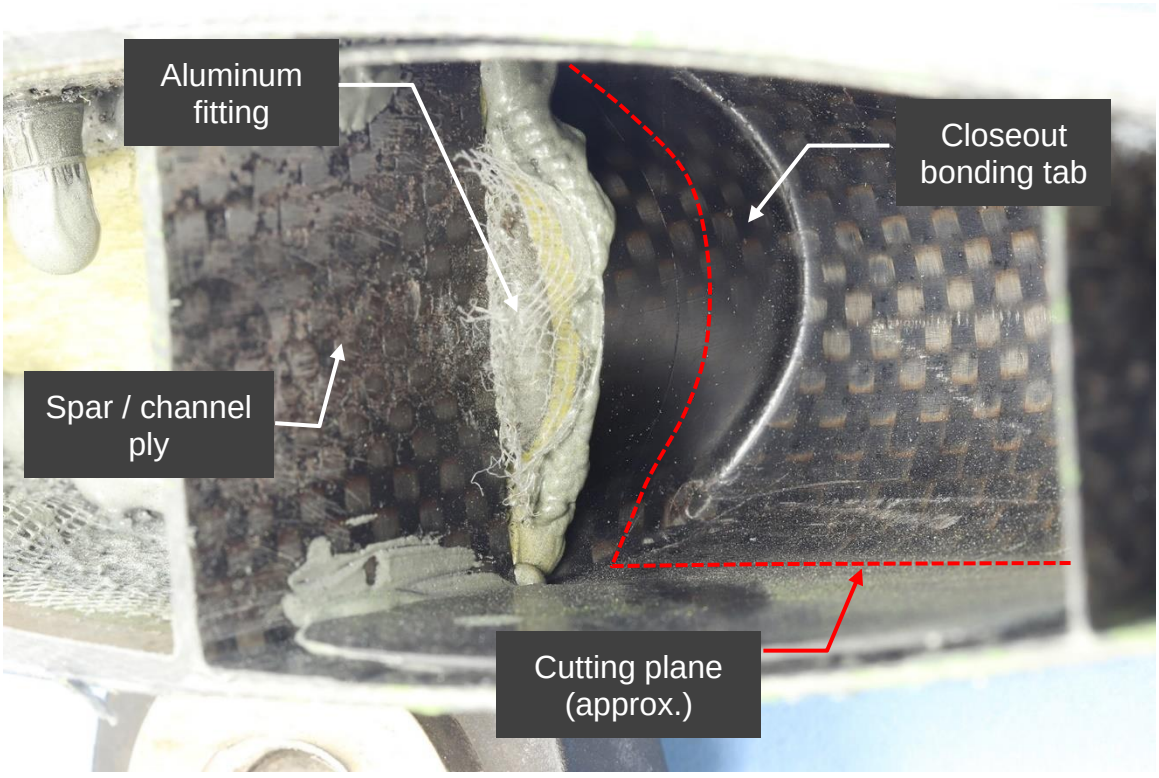

Figure 42. a) Sectioned inboard end of the RHR servo flap (S/N: 0565A) and b) view inside the sectioned end showing the closeout to aluminum fitting bond and the location of the cutting plane.

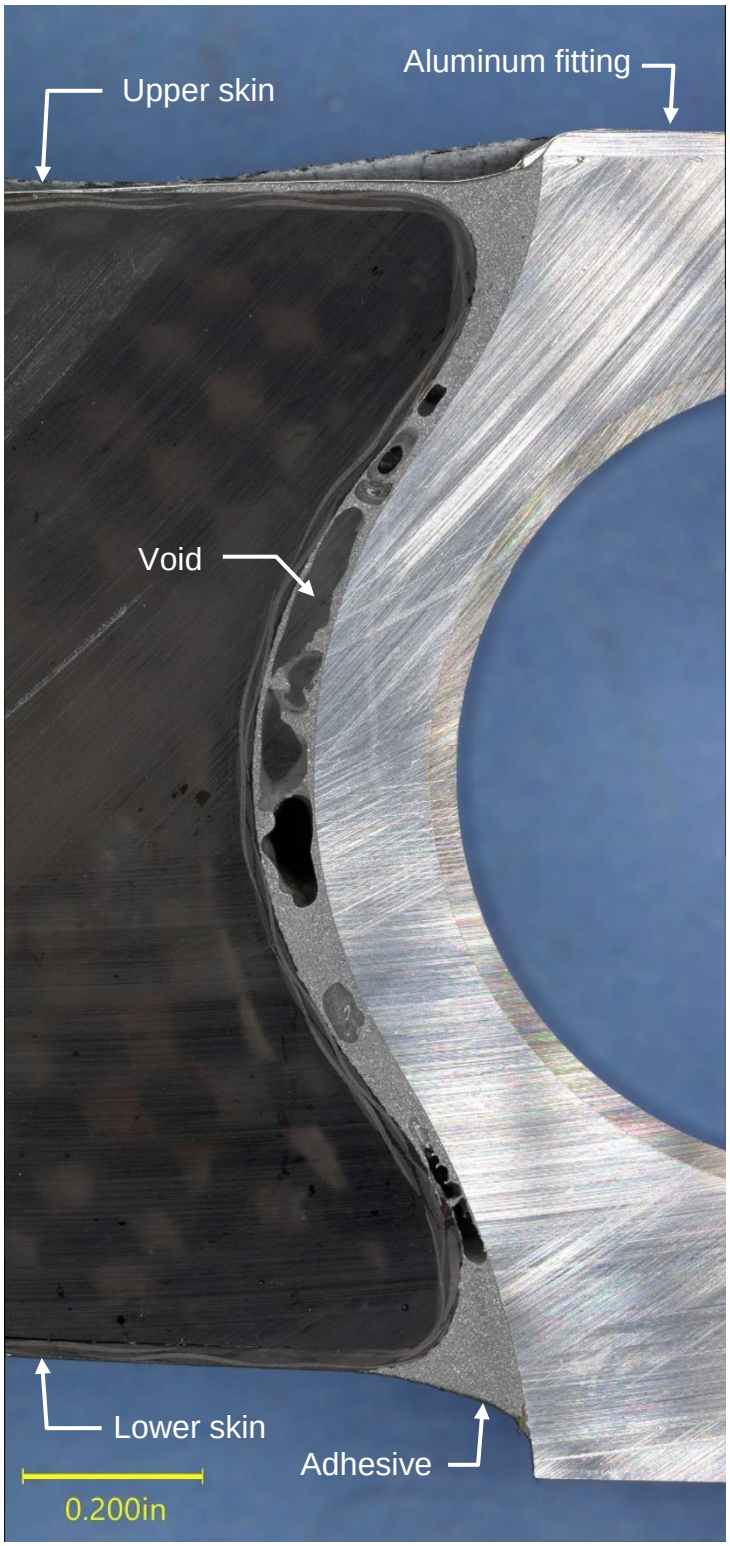

Figure 43. Cross section through LHR servo flap inboard closeout bond.

a) 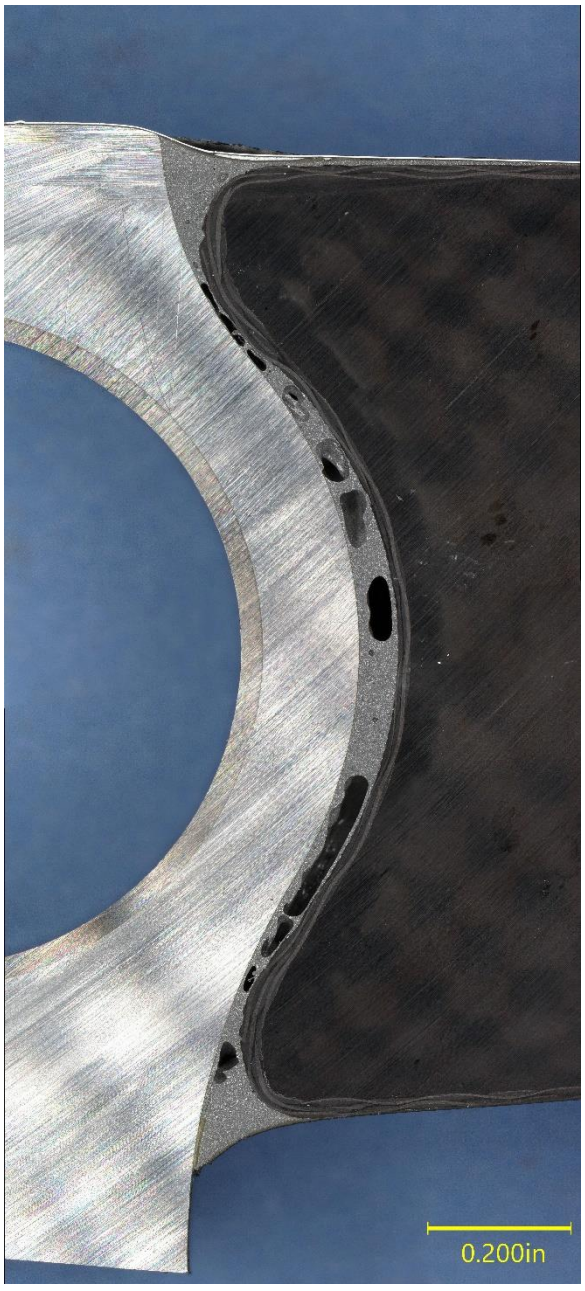

b) 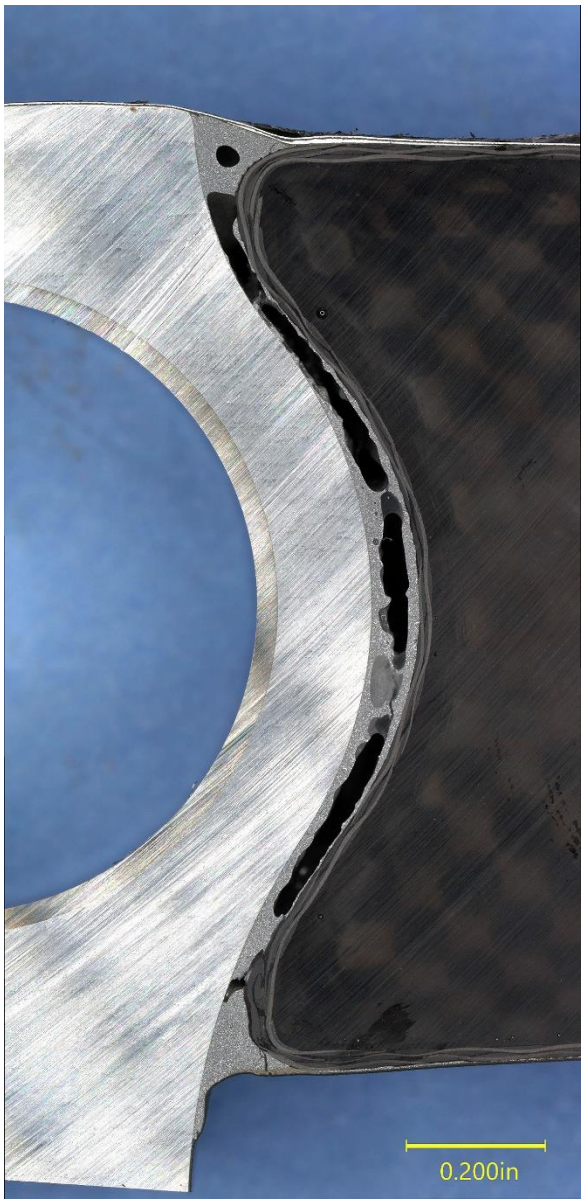

Figure 44. Cross sections through servo flap inboard closeout bonds: a) RHW and b) RHR.

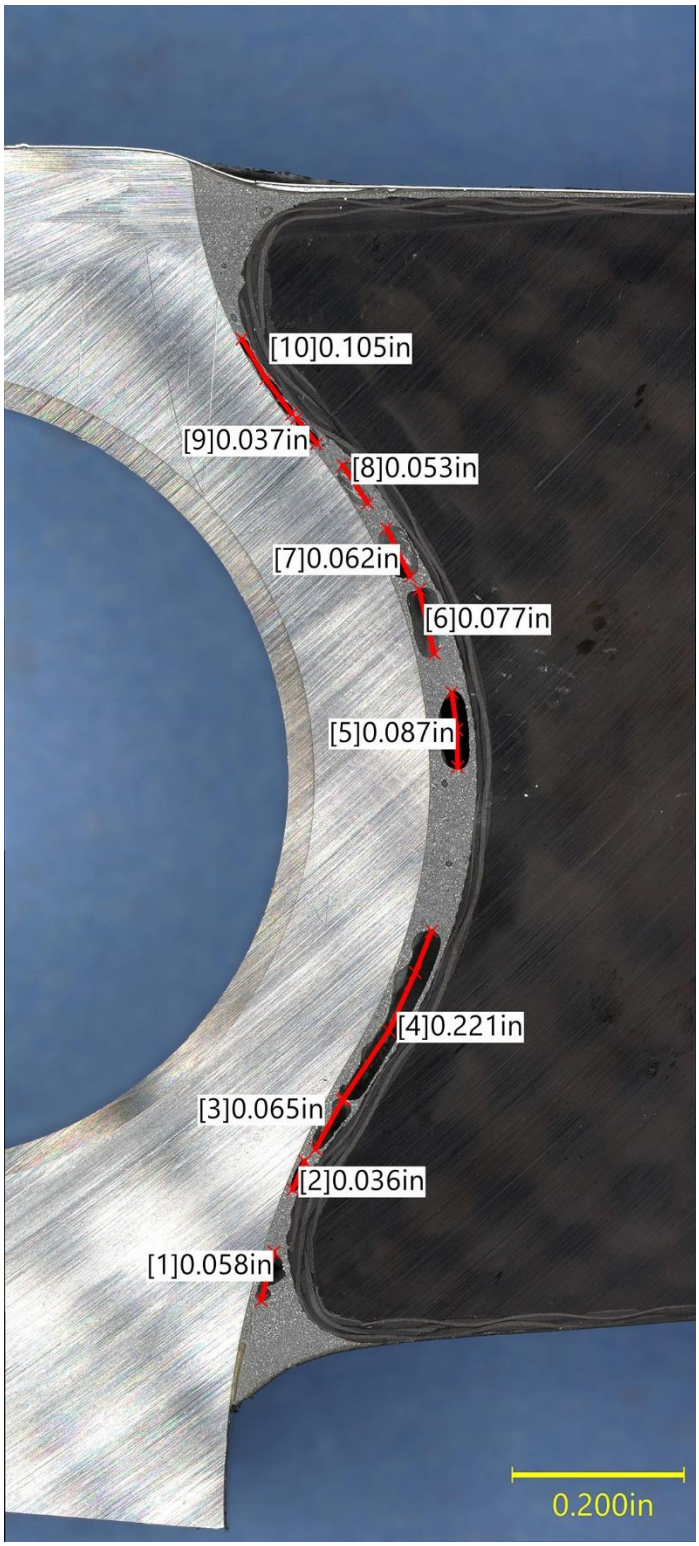

Figure 45. Example of void length measurement on the RHW servo flap inboard closeout bond.